Single cell transcriptomics reveals spatial and temporal dynamics of gene expression in the developing mouse spinal cord

Julien Delile*, Teresa Rayon, Manuela Melchionda, Amelia Edwards, James Briscoe‡, Andreas Sagner*‡

*These authors contributed equally

The Francis Crick Institute, 1 Midland Road, London NW1 1AT, UK

Correspondence: James Briscoe ‡ (james.briscoe@crick.ac.uk) or Andreas Sagner‡ (andreas.sagner@crick.ac.uk)

ABSTRACT

The coordinated spatial and temporal regulation of gene expression in the vertebrate neural tube determines the identity of neural progenitors and the function and physiology of the neurons they generate. Progress has been made deciphering the gene regulatory programmes responsible for this process, however, the complexity of the tissue has hampered the systematic analysis of the network and the underlying mechanisms. To address this, we used single cell mRNA sequencing to profile cervical and thoracic regions of the developing mouse neural tube between embryonic days (e)9.5-e13.5. We confirmed the data accurately recapitulates neural tube development, allowing us to identify new markers for specific progenitor and neuronal populations. In addition, the analysis highlighted a previously underappreciated temporal component to the mechanisms generating neuronal diversity and revealed common features in the sequence of transcriptional events that lead to the differentiation of specific neuronal subtypes. Together the data offer insight into the mechanisms responsible for neuronal specification and provide a compendium of gene expression for classifying spinal cord cell types that will support future studies of neural tube development, function, and disease.

INTRODUCTION

Neuronal circuits in the spinal cord receive and process incoming sensory information from the periphery, and control motor output to coordinate movement and locomotion (Goulding, 2009; Kiehn, 2016). The assembly of these circuits begins around embryonic day (e)9 in mouse embryos with the generation of distinct classes of neurons from proliferating progenitor cells located at defined positions within the neural tube. This is directed by signals emanating from the dorsal and ventral poles of the neural tube that partition progenitors into 13 transcriptionally distinct domains ordered along the dorsal ventral axis (Alaynick et al., 2011; Briscoe and Small, 2015; Jessell, 2000; Lai et al., 2016; Le Dréau and Martí, 2012). The gene expression programme of each progenitor domain determines the neuronal cell type it generates (Jessell, 2000; Lee and Pfaff, 2001). Neurons differentiate asynchronously from progenitors by undergoing a series of transcriptional changes that converts a proliferative progenitor into specific classes of neurons. Post-mitotic neurons subsequently further diversify into discrete subsets of physiologically distinct neuronal subtypes and commence formation of the circuitry characteristic of the spinal cord (Bikoff et al., 2016; Borowska et al., 2013; Goulding, 2009; Hayashi et al., 2018; Kiehn, 2016; Lu et al., 2015). Following the period of neurogenesis, which lasts until ~e13 in mouse, the remaining undifferentiated progenitors in the neural tube produce glia cells. This is accompanied by specific changes in gene expression in progenitors (Deneen et al., 2006; Kang et al., 2012; Stolt et al., 2003).

Although aspects of the gene regulatory network controlling neural tube patterning and neuronal differentiation have been characterised, there remain substantial gaps in our knowledge. It is unclear whether the complete catalogue of transcriptional regulators defining cell types has been established. Whether there are features in common between the mechanisms that promote the differentiation of distinct neuronal subtypes is not known. Similarly, the alterations in gene expression that accompany temporal changes in progenitor competence and cell type generation are poorly documented. In part this lack of knowledge is because, until recently, systematic expression profiling studies have been limited to the use of bulk dissected material. The spatial complexity of the neural tube and the lack of developmental synchrony between cells means that bulk studies do not have the resolution or sensitivity to provide detailed insight into gene expression or dynamics in specific cell lineages. Conversely, available single cell expression profiling studies of neural development have either focussed on *in vitro* derived neural progenitor cells (Briggs et al., 2017; Sagner et al., 2018), or analysed cells from post-natal animals or late stage embryos (Häring et al., 2018; Rosenberg et al., 2018; Sathyamurthy et al., 2018; Saunders et al., 2018; Zeisel et al., 2018).

To define systematically the complexity of cell types in the developing neural tube and determine the sequence of transcriptional events associated with neurogenesis, we performed single cell mRNA-seq analysis. We recovered 21465 cells from cervical and thoracic regions of the mouse neural tube across 5 developmental time points from e9.5 to e13.5. The data provide an unbiased classification of neural tube cell populations and their associated gene expression profiles. Using this dataset, we inferred the developmental trajectories leading to distinct neural cell fates and identified cohorts of co-regulated genes involved in specific developmental processes. This compendium of gene expression provides a molecular description of neural tube development and suggests testable hypotheses about neural tube development, function, and disease.

RESULTS

Assignment of transcriptomes to cell identities

To generate a gene expression atlas of the developing mouse neural tube, we used droplet-based scRNA-seq (10x Genomics Chromium) of microdissected cervical and thoracic regions of the spinal cord from mouse embryos between e9.5 and e13.5 (Fig 1A). We generated two replicates per timepoint for e9.5, e10.5 and e11.5. To compensate for the increase in size and cell number of the spinal cord, three replicates per timepoint were generated for e12.5 and e13.5 . In total, 41,025 cells were sequenced. After applying quality filters, a dataset of 38976 cells was retained for further analysis (7476 cells at e9.5, 6769 cells from e10.5, 6634 cells from e11.5, 8711 cells from e12.5, 9386 cells e13.5) (Fig S1A). The average number of UMIs and detected genes in these cells was similar between all samples analysed (Fig S1B,C).

We first allocated cells to different tissues based on the combinatorial expression of a curated gene list (Fig 1B). This allowed the classification of 33754 cells, 87% of the total cells. The remaining cells did not fall into any of the categories, potentially because of poorly resolved transcriptomes or because these cells were derived from other tissues of the embryo. Further subclustering the unclassified population did not reveal cell populations with spinal cord identity. We also estimated the rate at which the individual transcriptomes might represent more than one cell by assessing the proportion of transcriptomes displaying a gene expression signature of both neural and mesodermal tissue. This indicated that ~1% of the transcriptomes were from a mixture of neural and mesodermal cell types (Fig S1D).

Visualizing the resulting dataset with tSNE dimensionality reduction separated cells into multiple groupings that reflected the anticipated cell types (Fig 1D). Cells from replicate embryos, whether of the same or different sex, tended to intermingle within the embedding, suggesting minimal batch variation between embryos (Fig S1E,F). By contrast, there were obvious differences in the proportions of cell types from different timepoints. Most neurons were contained in the datasets obtained at later developmental stages (Figs 1D and S1F), consistent with the proportion of neurons increasing in the spinal cord over time (Kicheva et al., 2014). Conversely, most of the neural crest and mesoderm cells originated from e9.5 and e10.5 embryos (Figs 1D and S1F). This was due to the difficulty of cleanly dissecting the neural tube without accompanying adjacent tissue at these developmental stages.

As it was our aim to construct a spatiotemporal gene expression atlas of the developing spinal cord, we focused on the cells identified as spinal cord neural progenitors and neurons. A variety of molecular markers define different domains of progenitors and classes of neurons (Alaynick et al., 2011; Lai et al., 2016). Taking advantage of this, we generated a binary ‘knowledge matrix’ in which each progenitor domain and neuronal class is identified by the expression of a characteristic marker set (see Table S1). Notably, a specific cell type can be defined by more than one combination of marker gene expression patterns, which helps to capture certain subpopulations, such as early neurons that still partially express progenitor markers and have not yet fully activated their neuronal gene expression programmes. We then binarized the expression profiles of the defined marker genes in the transcriptome data and assigned each cell an identity from the knowledge matrix, using the minimal Euclidean distance between each transcriptome and cell type classes. Plotting the resulting average levels of marker gene expression for the assigned cell identities revealed the well-known patterns of

progenitor- and neuron-specific gene expression patterns (Fig 1C,E and S1G). We therefore conclude that the partitioning algorithm correctly assigns identities to the cells in our dataset.

Developmental dynamics of cell types

We hypothesized that sampling several thousand transcriptomes per time point would be sufficient to reconstruct the changes in domain sizes during development. Plotting the proportion of progenitors and neurons over time revealed a sharp decrease in the overall proportion of progenitors from >65% of cells at e9.5 to <15% of cells at e13.5 (Fig 2A). Previous work indicated that progenitor domain sizes in the spinal cord change over time (Kicheva and Briscoe, 2015; Kicheva et al., 2014). To test if the proportions of cells recovered from the assignment of cell identities accurately recapitulated the growth dynamics of the spinal cord, we compared with the quantification in Kicheva et al (2014). This revealed a close match (Fig 2E), allowing us to extend the analysis. Between e11.5 and e12.5, the rate of neurogenesis in the spinal cord appears to slow (Fig 2A,B); 24h later, at e13.5, the fraction of progenitors in dorsal domains decreased relative to ventral (Fig 2C,E). This is in line with the higher rate of neurogenesis in the dorsal spinal cord at e13.5 and the consequent depletion of progenitors (Gross et al., 2002; Lai et al., 2016; Müller et al., 2002).

We performed a similar analysis on the population dynamics of neuronal subtypes (Fig 2B,D). MNs are the most prominent class of neurons at early developmental stages (e9.5 and e10.5), consistent with the initially high differentiation rate of MN progenitors (Ericson et al., 1992; Kicheva et al., 2014; Novitch et al., 2001; Sagner et al., 2018) (Fig 2B,D). At later developmental stages (after e11.5), the proportions of inhibitory dI4 and excitatory dI5 neurons increased markedly (Fig 2D). This is explained by the expansion of the combined dp4/dp5 progenitor pool in the dorsal spinal cord at these stages and the extended phase of neurogenesis in the dorsal spinal cord that results in the formation of late born dI4 and dI5 neurons (also known as dIL_A and dIL_B) (Gross et al., 2002; Müller et al., 2002). Based on these observations, we conclude that the single cell transcriptomic atlas captures the domain dynamics of progenitor and neuronal populations.

Prediction of novel gene expression patterns

We sought to identify cell type specific expression patterns. Here the challenge is that different cell types are defined by overlapping combinations of gene expression. We constructed the list of all 2^{13} models of combinatorial patterns in progenitor domains (8192 combinations from 13 progenitor domains, including floor plate and roof plate) and we used these to identify genes with differential expression patterns. For each gene, the best fit model was selected and, after filtering by fold-change and significance level, we obtained a list of 102 combinations (Fig S2). The same procedure was then applied to the 12 neuronal populations (V3, MN, V2a, V2b, V1, V0, dI6, dI5, dI4, dI3, dI2, dI1) (Fig S3). From the 4096 combinatorial models obtained, we predicted 147 distinct patterns. We applied a conservative p-value cutoff of 10^{-9} to obtain a manageable list of candidates from the differential gene expression analysis; lowering this cutoff will extend the list of candidates to pursue in the future.

For further analysis, we first focused on genes encoding proteins involved in neurotransmitter biogenesis and release (Fig 3A). These identified the three main types of spinal cord neurons: cholinergic MNs, inhibitory GABAergic and glycinergic interneurons, and excitatory glutamatergic interneurons. These could be distinguished based on the expression of metabolic enzymes necessary for neurotransmitter production (e.g. Glutamatedecarboxylases Gad1 and Gad2) and specific

vesicular transporters e.g. Slc18a3 and Slc5a7 (vAcht and high-affinity choline transporter in MNs), Slc32a1 and Slc6a5 (vIAAT and Glycine Transporter 2 [GlyT2] in inhibitory interneurons) and Slc17a6 (vGlut2 in excitatory neurons). The analysis correctly predicted expression in the different neuronal populations: cholinergic MNs; inhibitory GABAergic and glycinergic dI4, V1 and V2b interneurons; and excitatory glutamatergic dI1, dI2, dI3, dI5, V2a, and V3 interneurons (Alaynick et al., 2011; Lai et al., 2016; Lu et al., 2015).

We next examined adhesion molecules (Fig 3A). In the spinal cord, differential cell adhesion is essential for the clustering of MNs into distinct pools (Demireva et al., 2011; Price et al., 2002) and differential adhesion mediated by Neurexins and Cerebellins is required for synapse formation and function (Südhof, 2017; Uemura et al., 2010). Interrogation of the data recovered 9 differentially expressed cell adhesion molecules (Cldn3, Cbln1, Cdh8, Pcdh11x, Clstn2, Pcdh7, Megf11, Nrxn3, Ret). Consistent with previous work, the analysis correctly predicted Pcdh7, Megf11 and Ret to be expressed in MNs (Catela et al., 2016; Hanley et al., 2016; Lin et al., 2012). We also found Nrxn3 to be specific for inhibitory neurons in the dI4, dI6, V1 and V2b domains. This pattern was anticorrelated with the expression pattern of Cbln1, which was expressed in excitatory dI3, dI5 and V3 neurons and MNs. Further investigation identified Nrxn1, as specifically expressed in excitatory neurons (dI1, dI2, dI3, dI5) (data not shown). This raises the possibility of a molecular adhesion code that distinguishes inhibitory and excitatory interneurons in the spinal cord, which might contribute to synaptogenesis during circuit formation.

To validate the inferred gene expression patterns, we focussed on Cldn3. Cldn3 encodes for a tight junction component (Morita et al., 1999) and was predicted to be specifically expressed in MNs before, but not after, e11.5 (Fig 3B). Assays confirmed this prediction (Fig 3C,D).

We next turned our attention to transcription factors (TFs) and searched for TFs that were differentially expressed between neuronal subtypes (Fig 3A). This recovered multiple TFs, many with well-established differential gene expression patterns, for example: Shox2 in V2a neurons (Dougherty et al., 2013; Hayashi et al., 2018); Foxp2 in V1 neurons (Morikawa et al., 2009; Stam et al., 2012); Lhx4 in MNs and V2a neurons (Lee and Pfaff, 2001; Sharma et al., 1998); Neurog3 and Uncx in V3 neurons (Carcagno et al., 2014; Sommer et al., 1996); and high-levels of Nr2f2 (also known as COUP-TF2), Nfia, Foxp1 and Creb5 in MNs (Dasen et al., 2008; Glasgow et al., 2017; Hanley et al., 2016; Lutz et al., 1994; Rousso et al., 2008). This analysis also suggested multiple previously unknown expression patterns of TFs, for example: expression of Hmx2 and Hmx3 in V1 and dI2 neurons; Sp9 in V1 neurons; and Bhlhe23 in dI2 neurons (Fig 3A).

For validation, we assayed Pou3f1 (also known as Oct6 or SCIP). This TF had previously been reported in multiple neuronal subtypes of spinal cord, e.g in MNs, V2a and V3 interneurons (Dasen et al., 2005; Francius et al., 2013), which we correctly identified. Our analysis also suggested that Pou3f1 is expressed in dorsal dI1-dI3 neurons (Fig 3A), which to our knowledge had not been described before. Assaying sections of embryonic spinal cord at e11.5 for Pou3f1, the dI1 marker Lhx2, and the dI3 marker Isl1, revealed broad expression of Pou3f1 in dorsal spinal cord neurons and colocalization between Pou3f1, Lhx2 and Isl1 (Fig 3E). We also detected Pou3f1+ cells not expressing Lhx2 nor Isl1, these are presumably dI2 neurons. Thus, the differential gene expression analysis correctly identified

the restricted expression patterns of multiple known genes and predicted novel patterns of expression.

Clustering of neurons predicts novel neuronal subtypes and transcriptional codes

The 11 neural progenitor domains (p0-p3, pMN, pd1-pd6) generate distinct classes of spinal neurons that further diversify into multiple subpopulations (Alaynick et al., 2011; Bikoff et al., 2016; Francius et al., 2013; Hayashi et al., 2018; Lai et al., 2016; Lu et al., 2015; Sweeney et al., 2018). Gene expression distinguishing subpopulations of neurons are well documented. To further probe the resolution of the dataset and identify novel components of the gene regulatory network involved in neuronal subtype specification, we performed hierarchical clustering independently on each neuronal class (Fig 4A-D and Fig S4). We first identified gene modules consisting of genes demonstrating concerted pattern of expression in each neuron class. The modules that showed differential expression in a class were used to perform hierarchical clustering and assign distinct subtype identities. This resulted in the identification of 59 subpopulations (Fig 4A). Of these, initial inspection indicated only two subpopulations were incorrectly assigned: one group consisting of poorly characterized neurons lacking any salient transcriptomic feature (clade MN.5) and a second population expressing late neural progenitor markers Sox9 and Fabp7 indicative of progenitor identity (clade V2a.5).

We focused on the identification of subpopulations of neurons in three ventral domains (V2a and V3 interneurons, and MNs) (Fig 4B-D). V3 interneurons have been previously shown to comprise at least 2 subtypes with distinct properties and settling positions in the spinal cord (Borowska et al., 2013; Francius et al., 2013; Goulding, 2009; Lu et al., 2015). In e12.5 mice, dorsal V3d neurons express Onecut TFs, while ventral V3v neurons express Olig3 (Francius et al., 2013). Hierarchical clustering of V3 neurons revealed at least 4 different subtypes (Fig 4B). Clade V3.1 consisted of newly differentiating V3 neurons that expressed the neurogenic markers Neurog3, Hes6 and Neurod4. Clade V3.2 was characterized by expression of Lhx1 and could be further subdivided into a Onecut2 positive and negative population. Clade V3.3 expressed the TFs Pou2f2, Zfhx2, Zfhx3, and Zfhx4, while cells in clade V3.4 expressed Neurod2, Neurod6 and Nfia/b/x. Furthermore, clades V3.3 and V3.4 are characterized by the expression of Pou3f1 and Olig3. Thus, the data correctly identified the different known types of V3 interneurons and predicted the existence of an additional Nfia/b/x and Neurod2/6 expressing subtype (Fig 4B).

After their generation, MNs diversify and organize into distinct columns and pools along the anterior-posterior axis of the spinal cord (Francius and Clotman, 2014; Jessell, 2000; Philippidou and Dasen, 2013; Stifani, 2014). Subclustering of the identified MNs revealed 6 clades (Fig 4C): Clades MN.2 and MN.3 comprised neurogenic progenitors, because cells in these clades expressed the progenitor markers Sox2, Hes5 and Olig2 (clade MN.3), or Hes6, Neurog2, and Neurod4 (clade MN.2) and did not express substantial levels of the vesicular acetylcholine transporter Slc18a3. The remaining four clades corresponded to more mature neurons. Clade MN.1 comprised early differentiated MNs characterized by the expression of the TF Pou2f2 and the tight junction component Cldn3; Median Motor Column (MMC) neurons and Phrenic Motor Column (PMC) neurons grouped in clade MN.4, which had high levels of Lhx3, Mecom, Pou3f1 and the PMC marker Alcam (Hanley et al., 2016; Stifani, 2014); and 2 clades (MN.6 and MN.7) of Foxp1-positive cells were identified. Clade MN.6 represented cervical Lateral Motor Column (LMC) neurons, expressing a gene module containing Aldh1a2 (also known as Raldh2) and the cervical Hox genes Hoxc4 and Hoxc5 (Fig 4C). Whereas Clade MN.7 comprised thoracic

preganglionic motor column (PGC) neurons. Clade MN.6 did not express Hoxc9, consistent with the limb level location of the LMC. By contrast, cells in clade MN.7 expressed higher levels of Hoxc9, characteristic of the thoracic regions (data not shown).

V2a interneurons have recently been shown to consist of two major subgroups that have different settling positions: a medial subgroup expressing Nfib and Neurod2 and a lateral subgroup that expresses Shox2 and Zfhx3 (Hayashi et al., 2018). Furthermore, the lateral subgroup seems to further diversify into subgroups labelled by Shox2 and Maf/Onecut TFs (Francius et al., 2013; Harris et al., 2018). Consistent with this, hierarchical clustering of the single cell transcriptome data revealed four major subtypes of V2a neurons (Fig 4D). Clade V2a.4 consisted mainly of newly differentiating neurons that expressed the neurogenic V2a markers Neurog1, Vsx1 and Hes6, but were not expressing the mature V2a marker Vsx2 (also known as Chx10). The three other neuronal subtypes were characterized by the expression of Neurod2, Nfia and Nfib (clade V2a.1); Shox2, Pou3f1, Pou2f2, Zfhx2, Zfhx3 and Zfhx4 (clade V2a.2); and Maf and Onecut2 (clade V2a.3). Thus, the data correctly predicted the different subtypes of V2a interneurons.

To test the accuracy of the transcriptome data, we assayed three predictions: the expression of Pou2f2 in V3; Nr2f1 (also known as COUP-TF1) in MNs; and Nkx6.2 in V2a interneurons (Fig 4B-D). Our analysis suggested that these TFs are expressed in specific subsets of neurons: Pou2f2 in a group of V3 interneurons that is complementary to the Olig3 and Onecut2 expressing populations; Nr2f1 in Foxp1+ MNs; and Nkx6.2 in a subpopulation of V2a interneurons that does not overlap with Shox2 and Nfib. Assaying expression in e11.5 and e12.5 cervical spinal cord (Fig 4E-G) confirmed each of the predictions. We therefore conclude that the spinal cord atlas provides sufficient resolution to detect distinct neuronal subtypes and implicates novel TFs in their specification.

Modular and temporal specification of neuronal identity

Having compiled a gene expression atlas encompassing multiple cell types and timepoints, we asked if we could use it to investigate the timing of neuronal subtype generation. We first identified sets of TFs that are used recurrently to define subpopulations of neurons in multiple domains (Fig 5). Modules containing Pou2f2 and Nfib were expressed in subpopulations of most neuronal classes (Fig 4B-D and Fig S4). Furthermore, Pou3f1, Onecut2 and Maf also demarcated subpopulations of multiple neuronal classes, consistent with the expression of these TFs in multiple types of neurons (Francius et al., 2013). The composition of the gene modules containing these TFs was well conserved between neuronal domains. The Pou2f2 gene module also contained Zfhx2, Zfhx3, and Zfhx4, in most cases. By contrast, the Nfib gene module often included Nfia, Nfix, Neurod2, Neurod6 and Tcf4. This raised the possibility that similar transcriptional programs mediate neuronal diversification in each of these domains.

We asked whether specific gene modules were induced at different timepoints in development. Examining the average expression level of Onecut2, Pou2f2, Zfhx3, Zfhx4, Nfia, Nfib, Neurod2 and Neurod6 for each neuronal class between e9.5 and e13.5 revealed a temporal stratification of neuronal subtypes that was conserved between domains (Fig 6A). The proportion of neurons that expressed Onecut2 and Pou2f2 peaked at early developmental stages (before e11.5), while Nfib and Neurod2 expression were induced at e12.5 or e13.5. This is consistent with prior observations: Onecut TFs have been shown to be expressed early in V1 and MNs (Roy et al., 2012; Stam et al., 2012) and Nfia/b are induced in MNs at later time points (Deneen et al., 2006; Kang et al., 2012). To test directly

for the temporal progression between subtypes, we first focussed on Onecut2 and Pou2f2. At e9.5 Onecut2 is expressed in neurons, whereas Pou2f2 was not detected at this stage (Fig 6B). At e10.5 expression of both markers was mutually exclusive, with Onecut2+ neurons typically occupying a more lateral position in the spinal cord than Pou2f2 neurons (Fig 6C). These observations are consistent with the single cell sequencing data and suggest a switch in neuronal subtype identity from Onecut2 to Pou2f2 between e9.5 and e10.5. Similar to Pou2f2 (Fig 6D), staining for Zfhx3 confirmed its expression in subsets of neurons at e10.5 (Fig S5A), whereas Nfib and Neurod2 were not expressed in neurons until after e11.5 (Fig 6E and S5B). Furthermore, Pou2f2 and Nfib were coexpressed with multiple domain specific markers at the respective stages (Fig S5C-E). Based on these observations, we conclude that neuronal subtype diversification in the spinal cord is at least partly driven by transcriptional programmes that are shared between multiple domains and sequentially induced in each of the domains. This suggests a temporal component to the specification of neuronal subtype identity that complements the well described spatial axis of patterning.

Reconstruction of the gene expression dynamics underlying neurogenesis

Finally, we turned out attention to the changes in gene expression that accompany the transition of progenitors to neurons. Single cell transcriptome analysis enables the reconstruction of gene expression dynamics along differentiation trajectories (Setty et al., 2016; Shin et al., 2015; Trapnell et al., 2014). To this end, we projected cells into a 2-dimensional space (Fig 7A) using Principal Component Analysis from a 100-dimensional space defined by a set of genes expressed in all DV domains during progenitor maturation and neurogenesis (Fig S6A). The first principal component aligned with neurogenesis, indicated by the down-regulation of Sox2 and up-regulation of Tubb3, hence we used PC1 coordinates as a pseudotemporal ordering for neurogenesis. We then reconstructed, independently for each domain, expression profiles of genes along pseudotime (Fig 7B). This predicted the expression changes in a set of 36 regionally patterned genes involved in neurogenesis (Fig 7C).

Examining gene expression changes as progenitors transitioned to neurons revealed the transient upregulation of several TFs. These included known neurogenic factors, including Atoh1, Neurog1 and Neurog2, and several domain specific TFs. In line with this, we recently demonstrated upregulation of Olig2 coincides with Neurog2 expression and neurogenesis in MN progenitors (Sagner et al., 2018). To test whether similar expression dynamics occur during neuronal differentiation in other progenitor domains, we first examined Olig3, which is expressed in the three most dorsal progenitor domains, dp1-dp3 (Müller et al., 2005). Differentiation of these progenitors into dI1-dI3 neurons depends on the expression of the proneural bHLH proteins: Atoh1 in dp1; Neurog1 in dp2; and Neurog2 in dp2 and dp3 progenitors (Lai et al., 2016). Plotting Olig3 expression dynamics along the differentiation trajectory from dp2 to dI2 neurons or dp3 to dI3 neurons revealed that the maximal expression of Olig3 coincided with the expression of Neurog1 and Neurog2 (Fig S6C,D). To test the specificity of the transient upregulation of Olig3, we examined the dynamics of Msx1 and Pax3. In contrast to Olig3, expression of both genes decreased monotonically during differentiation (Fig S6C,D). Assays of spinal cord sections revealed heterogeneity in Olig3 levels, with higher expression of Olig3 correlating with Neurog1 and Neurog2 expression and low levels of Msx1 (Fig S6F-H). These observations confirm that Olig3 expression is upregulated at the onset of neurogenesis and validated the predictions made by the pseudotemporal ordering.

Similar reconstruction of the p0 to V0 transition predicted that Dbx1 levels increase during neurogenesis (Fig 7D). Moreover, levels of the p3 marker Nkx2.2 were predicted to increase at the onset of neurogenesis (Fig S6B). Assays confirmed these predictions: Dbx1 levels were markedly elevated in Neurog1-positive p0 progenitors (Fig 7E), while Nkx2.2 levels were increased immediately adjacent to the p3 progenitor domain in Olig3-positive V3 neurons (Fig S6E). In both cases, upregulation was specific to the domain-specific TFs Dbx1 and Nkx2.2, but, consistent with the predictions made by the pseudo-temporal ordering, not seen for the more broadly expressed progenitor TFs Pax6 and Sox2 (Fig 7F and Fig S6E).

DISCUSSION

We have documented the transcriptional signatures of 21465 cells isolated from cervical and thoracic regions of the mouse neural tube during the developmental period that neuronal subtypes are generated. This sheds light on the changing gene expression profiles that characterise neural tube development and forms the basis of a molecular atlas of the developing mammalian spinal cord.

An atlas of spinal cord gene expression

The number of cells needed to generate a comprehensive atlas of a tissue depends on multiple factors including the number of cell types and the molecular differences between the cell types (Shekhar et al., 2016). There is a large diversity of cell types in the spinal cord. More than 50 distinct pools of MNs have been documented at limb levels of the spinal cord (Dasen et al., 2005; Landmesser, 2001; Philippidou and Dasen, 2013). Moreover, the combinatorial expression of nineteen TFs have been proposed to generate multiple subpopulations of V1 interneurons (Bikoff et al., 2016; Gabitto et al., 2016; Sweeney et al., 2018). Even though some of this diversity may arise at developmental stages later than those analysed in our study, it is likely that our analysis underestimates the diversity of cell types in the spinal cord. Increasing the number of cells sampled, particularly at e12.5 and e13.5, and improving the sensitivity of the methods to increase the complexity of the analysed transcriptomes might reveal further cell type diversity. In addition, neuronal subtypes vary along the rostral caudal axis of the neural tube (Hayashi et al., 2018; Philippidou and Dasen, 2013; Sweeney et al., 2018). We restricted our analysis to cervical and thoracic regions of the neural tube, hence our dataset will not represent cell types unique to lumbar and sacral spinal cord. Despite these limitations, we were able to detect all the progenitor populations and major neuronal subtypes described in cervical and thoracic regions of the spinal cord. Reassuringly, the proportions of the cell types recovered matched previously determined proportions in the spinal cord (Kicheva et al., 2014), suggesting that the methods did not substantially bias the composition of the transcriptomes recovered. Consistent with this, relatively small subclasses of several of the neuronal subtypes, such as V3, V2a and dI6 and specific subtypes of MNs including LMC and MMC MNs, were readily detected.

Although much progress has been made to reverse engineer the gene regulatory network responsible for pattern formation and cell fate specification in the neural tube (reviewed in Briscoe and Small, 2015; Lai et al., 2016), it remains incomplete. This study makes available detailed information on the transcriptional state of the entire population of neural tube cells and will likely accelerate efforts to comprehensively map the transcriptional network. To assemble the single-cell transcriptomic atlas,

we took advantage of the extensive prior knowledge of gene expression to analyse and organise the transcriptome data (Fig 1C,E). This allowed us to expand the molecular description of cell types and define new subdivisions of neurons. Importantly, experimental assays corroborated the transcriptome predictions, suggesting that the atlas is a generally faithful representation of gene expression in the spinal cord. Further mining the dataset will likely implicate additional TFs in the neural tube gene regulatory network and refine the molecular classification of cell types.

Temporal specification of neuronal subtype identity

The data highlighted a previously underappreciated systematic temporal component to the specification neuronal subtype identity in the neural tube. Temporal mechanisms, in which a sequence of TFs is expressed in succession to determine distinct neuronal identities, are well established in cortical neurogenesis and Drosophila neuroblasts (Holguera and Desplan, 2018). In the spinal cord, the birth date of spinal neurons has been shown to correlate with subtype identity and functional properties in several specific cases (Hayashi et al., 2018; Hollyday and Hamburger, 1977; Sockanathan and Jessell, 1998; Stam et al., 2012; Tripodi et al., 2011). Whether this is a consequence of a global patterning strategy that involves temporally organised changes in gene expression has been unclear. Analysis of the single cell transcriptome dataset revealed a set of gene expression modules activated synchronously at characteristic developmental timepoints in multiple neuronal classes. This raises the possibility of a coordinated temporal transcriptional programme that subdivides neuronal classes based on their time of generation. Such a mechanism would operate in parallel to the spatial patterning mechanisms and provide an opportunity to increase the molecular and functional diversity of cell types generated in the neural tube.

The coordinated induction of gene modules in multiple neuronal subtypes might result from a global transcriptional change in the neural progenitors from which they are generated. In the spinal cord, a transcriptional cascade of Sox9 and Nfia/b in progenitors underlies the progressive activation of gliogenesis (Deneen et al., 2006; Kang et al., 2012; Stolt et al., 2003). Sox9 expression begins between e9.5 and e10.5, while Nfia/b is expressed from e11.5 (Deneen et al., 2006; Stolt et al., 2003). However, the forced expression of these TFs does not repress neurogenesis and neurons continue to be produced for a considerable period after their expression commences (Deneen et al., 2006). The onset of expression of Sox9 coincides with the switch of V1 neurons from Renshaw cells (Onecut expressing) to Foxp2 expressing neurons (Kang et al., 2012; Stam et al., 2012; Stolt et al., 2003). This raises the possibility that the induction of TFs, such as Sox9 and Nfia/b, changes the competency of neural progenitors to give rise to specific neuronal subtypes and that neural progenitors within a single domain are different over time. In this view, the same mechanism responsible for the activation of gliogenesis in neural progenitors serves as a mechanism to generate neuronal diversity in a coordinated manner throughout the spinal cord. Experiments are required to test this and investigate whether similar principles apply to other regions of the nervous system.

Extrinsic signals may contribute to the temporal stratification of neuronal subtypes. Retinoic acid promotes Renshaw cell identity in V1 neurons (Hoang et al., 2018), and the timepoint of their generation correlates with expression of the RA-synthesizing enzyme Aldh1a2 in the adjacent somites (Niederreither et al., 1997). Thus, besides promoting neurogenesis (Novitch et al., 2003), somite-derived RA may be a determinant for early Onecut-positive neuronal subtypes. Another candidate for mediating the temporal progression of neuronal subtypes is TGFβ signalling, which has been shown

to suppress early born neuronal identities in favour of later born cell types in multiple regions of the nervous system (Dias et al., 2014). Lastly, we observed the expression of FGF ligands in multiple neuronal subtypes, while neural progenitors at later stages up-regulated FGF receptor3 (Fgfr3) and FGF-binding protein 3 (Fgfbp3) (Gonzalez-Quevedo et al., 2010; Kang et al., 2012). Thus, multiple secreted signalling molecules may determine into which neuronal subtypes progenitors in the spinal cord differentiate at specific timepoints.

Dynamics of gene expression during neurogenesis

We have previously demonstrated that upregulation of Olig2 precedes MN formation in vivo and in vitro (Sagner et al., 2018). Pseudotemporal ordering of the progenitor to neuron transition for multiple progenitor domains predicted the transient upregulation of domain specific TFs during neurogenesis (Fig 7C). We confirmed this experimentally for Olig3 in dp2/3, Dbx1 in p0 and Nkx2.2 in p3 progenitors (Fig 7D,E and Fig S6A-D). We propose that the upregulation of domain-specific TFs prior to neurogenesis reinforces neuronal specificity during differentiation (Fig 7G). At early developmental stages, morphogen gradients establish discrete domains of progenitor identities along the DV axis by inducing distinct TFs (Alaynick et al., 2011; Briscoe and Small, 2015; Le Dréau and Martí, 2012). These TFs form a gene regulatory network that establishes progenitor identities by repressing not only adjacent progenitor identities but also a wide range of alternative fates (Kutejova et al., 2016; Nishi et al., 2015). The dynamics of the gene regulatory network results in progenitors undergoing a succession of changes in TF expression, mediated by repressive interactions, during their specification. The lower levels of domain specific TFs in progenitors, prior to neurogenesis, might therefore ensure sensitivity to morphogen inputs and facilitate cell state transitions in response to morphogen inputs. Such a mechanism, however, could be prone to the generation of mixed neuronal identities as neurogenesis commences (Ericson et al., 1996). The upregulation of the domain specific TFs during neurogenesis might serve to consolidate the appropriate identity and to prevent the initiation of a mixed neuronal identity during differentiation. Thus, the upregulation of domain specific TFs during neuronal differentiation could provide a means to enhance the fidelity of spinal cord patterning.

In conclusion, we document the molecular diversity and cellular composition of the developing mouse neural tube. The data allows the identification of genes and regulatory modules that define specific cell types. The analysis suggests a temporal axis contributing to neuronal diversity that accompanies the well characterised spatial patterning of neural progenitors. Together, the data provide new opportunities to understand gene function and to genetically target cells for visualization or manipulation and will support efforts to understand the structure and function of the healthy as well as diseased or damaged spinal cord.

MATERIALS AND METHODS

Animal welfare

Animal experiments in the Briscoe lab were performed under UK Home Office project licenses (PD415DD17) within the conditions of the Animal (Scientific Procedures) Act 1986. Outbred UKCrl:CD1 (ICR) (Charles River) mice were used for this study.

Immunofluorescent staining and recording of spinal cord sections

Mouse spinal cord tissues were fixed in 4% paraformaldehyde (Thermo Scientific) in PBS, cryoprotected in 15% sucrose, embedded in gelatine, and 14 µm sections taken. A complete list of primary antibodies including manufacturer and used dilutions is provided in Table S3. Secondary antibodies used throughout this study were raised in donkey (Life Technologies; Jackson Immunoresearch; Sigma; Biotium). Alexa488 and Alexa568 conjugated antibodies were used at 1:1000 dilution; Alexa647 conjugated antibodies were used at 1:500 and CF405M conjugated secondary antibodies at 1:250.

Images were acquired on a Zeiss Imager.Z2 microscope equipped with an Apotome.2 structured illumination module and a 20x air objective (NA=0.75). 5 phase images were acquired for structured illumination. Z-stacks consisted of 8 sections separated by 1 µm were acquired. Individual optical slices are shown. If required, adjacent images were acquired with 5-10% of overlap and stitching was performed in Fiji using the “Grid/Collection stitching” plugin (Preibisch et al., 2009).

Sample preparation for single cell RNA sequencing

Outbred CD1 females were timed mated to generate mouse embryos of the specified stages. The morning of the vaginal plug was defined as embryonic day (e)0.5. For neural tube dissection, cervical and thoracic sections of single mouse embryos were dissected in Hanks Balanced Solution without calcium and magnesium (HBSS, Life Technologies 14185045) supplemented with 5% heat-inactivated fetal bovine serum (FBS). The samples were then incubated on FACS max cell dissociation solution (Amsbio T200100) with 10X Papain (30U/mg Sigma10108014001) for 11min at 37°C to dissociate the cells. To generate a single cell suspension, samples were transferred to HBSS, with 5%FBS, rock inhibitor (Y-27632 10uM, Stem Cell Technologies), and 1X non-essential amino acids (Thermo Fisher 11140035), disaggregated through pipetting, and filtered once through 0.35um filters and once through 0.20um strainers (Miltenyi Biotech 130-101-812). Quality control was assayed by measuring live/cell death, cell size and number of clumps. Samples with a viability above 65% were used for sequencing. 10,000 cells per sample were loaded for sequencing.

Single cell generation, cDNA synthesis and library construction

A suspension of 10,000 single cells was loaded onto the 10X Genomics Single Cell 3' Chip, and cDNA synthesis and library construction performed as per the manufacturer's protocol for the Chromium Single Cell 3' v2 protocol (10X Genomics; PN-120233). cDNA amplification involved 12 PCR cycles.

Nucleic acid sequencing protocol

Libraries for the samples were multiplexed so that the number of reads matched one lane per sample, and sequenced on an Illumina HiSeq 4000 using 100bp paired-end runs. Libraries were generated in independent runs for the different samples and for different time points.

Alignment and preparation of scRNA-seq data

Demultiplexing, alignment, filtering, as well as barcode and UMI counting were performed using Cell Ranger (version 2.2.0, 10X Genomics, under default settings), which uses STAR aligner. The aggregated gene-barcode matrix was normalized by subsampling reads from higher-depth libraries until all samples had an equal number of confidently mapped reads per cell. Further analysis was performed using R.

Quality filtering

We excluded cells having more than 6% UMI counts associated with mitochondrial genes and expressing less than 500 genes.

Data analysis

We partitioned cells into 13 progenitor and 12 neuronal populations using the following two-step strategy. First, we determined the global cell identities by associating each cell to the closest target population state defined by a list of known marker genes (Fig 1B). The binarized levels were obtained using a threshold of 2 UMI counts and cell-to-target distances were calculated by Euclidean distance. Second, each progenitor and neuronal population was further partitioned using the same approach using the list of marker genes shown on Fig 1C,E.

Combinatorial testing for differential expression

To classify the whole transcriptome by categories of spatial dorsal-ventral patterns, we performed a series of differential expression tests. The analysis was performed independently on progenitors and neurons. In both cases, the procedure was identical: for each gene, 2^N-2 (resp. N=13 for progenitor domains and N=12 for neuronal domains) approximate χ^2 likelihood-ratio tests were run between a null hypothesis that models gene expression as a function of a single sample (no predictor) versus an alternative hypothesis modeling gene expression as a function of two samples; the “positive” sample being one of the potential population combinations and the “negative” sample the complementary combination. Hence, all combinations were tested. The tests were run using Monocle (version 2.6.4) *differentialGeneTest* function with gene level distributions modeled as negative binomial distributions with fixed variance (option *expressionFamily=negbinomial.size(),* as recommended for UMI datasets). Each gene was then associated with the population combination having obtained the highest likelihood. The gene list was trimmed using significance (P value < 10^{-9}) and fold-change (log2-fc > 2) cutoffs. We also ensured that the remaining genes had a minimal average level of expression (0.2 UMI) and a ratio of expressed cells (10% in progenitors, 8% in neurons) in the positive samples.

The gene sets highlighted in Figure 3A were obtained by intersecting the differentially expressed genes with the following GO terms: GO:0098609 for cell-cell adhesion and GO:0006836 for neurotransmitter transport.

Subclustering of neuronal populations

To investigate the diversity of neuronal subtypes, the neuronal population was subdivided into 12 dorsal-ventral domains (see above). Because only a few dI6 neurons were recovered (95 out of 16450 neurons), we excluded this domain for the following subclustering analysis. For each of the remaining 11 domains, we pooled together the associated neuronal cells and applied the following procedure:

1. Unbiased identification of transcriptomic features

We reasoned that relevant transcriptomic features involve interacting genes demonstrating concerted patterns of expression. From the initial set of ~5000 expressed genes, we selected the genes that showed highest Spearman correlation with at least three other genes, lowering the correlation cutoff until ~2000 genes were retained. These genes were then grouped and further filtered with the following 3-step iterative method:

a. The remaining genes were grouped into gene modules by performing a hierarchical clustering using the Spearman dissimilarity matrix of the UMI counts and Ward's agglomeration criterion. The number of modules were set heuristically to 200 to produce compact and homogeneous groupings.
b. A first filtering criterion was applied to test whether enough cells were expressing the genes comprising the gene module. For each cell, we obtained an average expression level per module by averaging the z-scored log-transformed expression levels of all genes belonging to the module. These gene module averaged levels were then binarized independently by using a parameter-free adaptive thresholding method (R function *binarize.array()* from the ArrayBin package). A cell was considered to express a gene module if the associated Boolean value was true. Modules which were expressed in fewer than five cells were excluded.
c. A second filtering criterion was then applied to test whether cells were expressing the gene module with consistently high levels over most of the genes in the module. We binarized the z-scored log-transformed expression levels of all the remaining genes independently. Then, for each module, we calculated the ratio of Boolean values in cells expressing the module (as defined in b.). We excluded modules where less than 40% of these Boolean values were true.

The iterative loop was terminated when the number of gene modules converged, i.e. when no gene module was excluded in the last iteration. A summary table indicating the number of expressed genes, correlated genes, unbiasedly-identified genes, and gene modules per domain is available in Table S4.

2. Curated selection of the relevant features and neuron type clustering

The gene modules were carefully scrutinized using a list of known neuronal marker genes. We isolated a list of curated gene modules related to neuronal identities (Table S2 and gene module counts in Table S4). In each domain independently, a variable number of identities were obtained by performing

a hierarchical clustering of the cells, using Euclidean distances between z-scored log-transformed expression levels of the remaining genes.

Neuronal trajectories and Pseudotime reconstruction

To project the whole neural dataset into a space that reveals cell state transitions during neurogenesis and progenitor maturation, we aimed at identifying a set of genes with similar dynamics in each dorsal-ventral domain. In order to reduce any bias toward overrepresented populations, we used a resampled dataset containing approximately the same number of cells per timepoint and dorsal-ventral domain. The unbiased gene module identification pipeline described above was used to identify 200 gene modules of concerted patterns of expression in the resampled dataset. Among them, 4 modules were retained as they comprised, respectively, the pan-progenitor marker Sox2, the pan-neuronal marker Tubb3, the early progenitor marker Lin28a and the late progenitor marker Fabp7 (114 genes). An extra step was taken to ensure that no dorsal-ventral bias occurred in the remaining genes by testing for differential expression in response to their DV position (Monocle 2.6.4, *differentialGeneTest* function, p-value < 5e-15). 14 genes were excluded and 100 retained (Fig S6A). After taking the log of the normalized UMI counts ("median ratio" normalization method), Principal Component Analysis was then applied to the 100-dimensional resampled dataset. The resulting PC1-PC2 plane was then populated by multiplying the whole (log-normalized) neural dataset by the eigenvector matrix. Neurogenic pseudotime orderings of each cell were mapped to the PC1 coordinates.

Finally, we reconstructed, independently for each domain, smoothed profiles of gene expression along pseudotime by fitting spline curves (Monocle 2.6.4, *genSmoothCurves* with 3 degree of freedom). Each profile obtained with less than 20 expressed cells was set to zero.

ACKNOWLEDGEMENTS

We are grateful to the Advanced Sequencing and Scientific Computing Facilities of the Francis Crick Institute. We acknowledge Monica Tambalo for sharing her protocol for single-cell embryo dissociation. We thank Bennett Novitch, Thomas Jessell, Susan Morton, Thomas Müller, Carmen Birchmeier and Francois Guillemot for kindly sharing antibodies. A.S. receives funding from an HFSPO postdoctoral fellowship (LTF000401/2014-L), T.R. received funding from an EMBO long term fellowship (ALTF 328-2015). This work was supported by the Francis Crick Institute, which receives its core funding from Cancer Research UK (FC001051), the UK Medical Research Council (FC001051), and Wellcome (FC001051); and by the European Research Council (ERC) under the European Union's Horizon 2020 research and innovation programme (Grant Number 742138).

AUTHOR CONTRIBUTIONS

Conceptualization, J.D., T.R., J.B., A.S.; Methodology, J.D., T.R., A.S; Software, J.D.; Formal Analysis, J.D.; Resources, A.E. and M.M.; Writing – Original Draft, J.D., T.R., J.B., A.S.; Writing – Review and Editing, J.D., T.R., M.M., J.B., A.S., Visualization, J.D., T.R., A.S., Supervision, J.B., Funding Acquisition, T.R., J.B., A.S.

Data availability

Single cell RNA sequencing data are available via ArrayExpress (http://www.ebi.ac.uk/arrayexpress/experiments/E-MTAB-7320). All other relevant data has been uploaded as Supporting information files.

Source code availability

The R analysis script developed for this paper is available at https://github.com/juliendelile/MouseSpinalCordAtlas.

REFERENCES

Alaynick, W. A., Jessell, T. M. and Pfaff, S. L. (2011). SnapShot: Spinal cord development. *Cell* **146**, 178.e1.

Bikoff, J. B., Gabitto, M. I., Rivard, A. F., Drobac, E., Machado, T. A., Miri, A., Brenner-Morton, S., Famojure, E., Diaz, C., Alvarez, F. J., et al. (2016). Spinal Inhibitory Interneuron Diversity Delineates Variant Motor Microcircuits. *Cell* **165**, 207–219.

Borowska, J., Jones, C. T., Zhang, H., Blacklaws, J., Goulding, M. and Zhang, Y. (2013). Functional Subpopulations of V3 Interneurons in the Mature Mouse Spinal Cord. *J. Neurosci.* **33**, 18553–18565.

Briggs, J. A., Li, V. C., Lee, S., Woolf, C. J., Klein, A. and Kirschner, M. W. (2017). Mouse embryonic stem cells can differentiate via multiple paths to the same state. *Elife* **6**, 1–31.

Briscoe, J. and Small, S. (2015). Morphogen rules: design principles of gradient-mediated embryo patterning. *Development* **142**, 3996–4009.

Carcagno, A. L., Di Bella, D. J., Goulding, M., Guillemot, F. and Lanuza, G. M. (2014). Neurogenin3 Restricts Serotonergic Neuron Differentiation to the Hindbrain. *J. Neurosci.* **34**, 15223–15233.

Catela, C., Shin, M. M., Lee, D. H., Liu, J.-P. and Dasen, J. S. (2016). Hox Proteins Coordinate Motor Neuron Differentiation and Connectivity Programs through Ret/Gfrα Genes. *Cell Rep.* **14**, 1901–15.

Clevers, H., Rafelski, S., Elowitz, M. and Lein, E. (2017). What Is Your Conceptual Definition of "Cell Type" in the Context of a Mature Organism? *Cell Syst.* **4**, 255–259.

Dasen, J. S., Tice, B. C., Brenner-Morton, S. and Jessell, T. M. (2005). A Hox Regulatory Network Establishes Motor Neuron Pool Identity and Target-Muscle Connectivity. *Cell* **123**, 477–491.

Dasen, J. S., De Camilli, A., Wang, B., Tucker, P. W. and Jessell, T. M. (2008). Hox Repertoires for Motor Neuron Diversity and Connectivity Gated by a Single Accessory Factor, FoxP1. *Cell* **134**, 304–316.

Demireva, E. Y., Shapiro, L. S., Jessell, T. M. and Zampieri, N. (2011). Motor neuron position and topographic order imposed by β- And γ-catenin activities. *Cell* **147**, 641–652.

Deneen, B., Ho, R., Lukaszewicz, A., Hochstim, C. J., Gronostajski, R. M. and Anderson, D. J. (2006). The Transcription Factor NFIA Controls the Onset of Gliogenesis in the Developing Spinal Cord. *Neuron* **52**, 953–968.

Dias, J. M., Alekseenko, Z., Applequist, J. M. and Ericson, J. (2014). Tgfβ signaling regulates temporal neurogenesis and potency of neural stem cells in the CNS. *Neuron* **84**, 927–939.

Dougherty, K. J., Zagoraiou, L., Satoh, D., Rozani, I., Doobar, S., Arber, S., Jessell, T. M. and Kiehn, O. (2013). Locomotor Rhythm Generation Linked to the Output of Spinal Shox2 Excitatory Interneurons. *Neuron* **80**, 920–933.

Ericson, J., Thor, S., Edlund, T., Jessell, T. M. and Yamada, T. (1992). Early stages of motor neuron differentiation revealed by expression of homeobox gene Islet-1. *Science (80-.).* **256**, 1555 LP-1560.

Ericson, J., Morton, S., Kawakami, A., Roelink, H. and Jessell, T. M. (1996). Two critical periods of Sonic Hedgehog signaling required for the specification of motor neuron identity. *Cell* **87**, 661–673.

Francius, C. and Clotman, F. (2014). Generating spinal motor neuron diversity: A long quest for neuronal identity. *Cell. Mol. Life Sci.* **71**, 813–829.

Francius, C., Harris, A., Rucchin, V., Hendricks, T. J., Stam, F. J., Barber, M., Kurek, D., Grosveld, F. G., Pierani, A., Goulding, M., et al. (2013). Identification of Multiple Subsets of Ventral Interneurons and Differential Distribution along the Rostrocaudal Axis of the Developing Spinal Cord. *PLoS One* **8**, e70325.

Gabitto, M. I., Pakman, A., Bikoff, J. B., Abbott, L. F., Jessell, T. M. and Paninski, L. (2016). Bayesian Sparse Regression Analysis Documents the Diversity of Spinal Inhibitory Interneurons. *Cell* **165**, 220–233.

Glasgow, S. M., Carlson, J. C., Zhu, W., Chaboub, L. S., Kang, P., Lee, H. K., Clovis, Y. M., Lozzi, B. E., McEvilly, R. J., Rosenfeld, M. G., et al. (2017). Glia-specific enhancers and chromatin structure regulate NFIA expression and glioma tumorigenesis. *Nat. Neurosci.* **20**, 1520–1528.

Gonzalez-Quevedo, R., Lee, Y., Poss, K. D. and Wilkinson, D. G. (2010). Neuronal Regulation of the Spatial Patterning of Neurogenesis. *Dev. Cell* **18**, 136–147.

Goulding, M. (2009). Circuits controlling vertebrate locomotion: moving in a new direction. *Nat. Rev. Neurosci.* **10**, 507–518.

Gross, M. K., Dottori, M. and Goulding, M. (2002). Lbx1 specifies somatosensory association interneurons in the dorsal spinal cord. *Neuron* **34**, 535–549.

Hanley, O., Zewdu, R., Cohen, L. J., Jung, H., Lacombe, J., Philippidou, P., Lee, D. H., Selleri, L. and Dasen, J. S. (2016). Parallel Pbx-Dependent Pathways Govern the Coalescence and Fate of Motor Columns. *Neuron* **91**, 1005–1020.

Häring, M., Zeisel, A., Hochgerner, H., Rinwa, P., Jakobsson, J. E. T., Lönnerberg, P., La Manno, G., Sharma, N., Borgius, L., Kiehn, O., et al. (2018). Neuronal atlas of the dorsal horn defines its architecture and links sensory input to transcriptional cell types. *Nat. Neurosci.* **21**, 869–880.

Harris, A., Masgutova, G., Collin, A. and Toch, M. (2018). Onecut factors and Pou2f2 regulate diversification and migration of V2 interneurons in the mouse developing spinal cord.

Hayashi, M., Hinckley, C. A., Driscoll, S. P., Moore, N. J., Levine, A. J., Hilde, K. L., Sharma, K. and Pfaff, S. L. (2018). Graded Arrays of Spinal and Supraspinal V2a Interneuron Subtypes Underlie Forelimb and Hindlimb Motor Control. *Neuron* 1–16.

Hoang, P. T., Chalif, J. I., Bikoff, J. B., Jessell, T. M., Mentis, G. Z. and Wichterle, H. (2018). Subtype Diversification and Synaptic Specificity of Stem Cell-Derived Spinal Interneurons. *Neuron* **100**, 135–149.e7.

Holguera, I. and Desplan, C. (2018). Neuronal specification in space and time. *Science (80-.).* **362**, 176–180.

Hollyday, M. and Hamburger, V. (1977). An autoradiographic study of the formation of the lateral motor column in the chick embryo. *Brain Res.* **132**, 197–208.

Jessell, T. M. (2000). Neuronal specification in the spinal cord: inductive signals and transcriptional codes. *Nat Rev Genet* **1**, 20–29.

Kang, P., Lee, H. K., Glasgow, S. M., Finley, M., Donti, T., Gaber, Z. B., Graham, B. H., Foster, A. E., Novitch, B. G., Gronostajski, R. M., et al. (2012). Sox9 and NFIA Coordinate a Transcriptional Regulatory Cascade during the Initiation of Gliogenesis. *Neuron* **74**, 79–94.

Kicheva, A. and Briscoe, J. (2015). Developmental Pattern Formation in Phases. *Trends Cell Biol.* **25**, 579–91.

Kicheva, A., Bollenbach, T., Ribeiro, A., Valle, H. P., Lovell-Badge, R., Episkopou, V. and Briscoe, J. (2014). Coordination of progenitor specification and growth in mouse and chick spinal cord. *Science* **345**, 1254927.

Kiehn, O. (2016). Decoding the organization of spinal circuits that control locomotion. *Nat. Rev. Neurosci.* **17**, 224–238.

Kutejova, E., Sasai, N., Shah, A., Gouti, M. and Briscoe, J. (2016). Neural Progenitors Adopt Specific Identities by Directly Repressing All Alternative Progenitor Transcriptional Programs. *Dev. Cell* **36**, 639–653.

Lai, H. C., Seal, R. P. and Johnson, J. E. (2016). Making sense out of spinal cord somatosensory development. *Development* **143**, 3434–3448.

Landmesser, L. T. (2001). The acquisition of motoneuron subtype identity and motor circuit formation. *Int. J. Dev. Neurosci.* **19**, 175–182.

Le Dréau, G. and Martí, E. (2012). Dorsal-ventral patterning of the neural tube: A tale of three signals. *Dev. Neurobiol.* **72**, 1471–1481.

Lee, S. K. and Pfaff, S. L. (2001). Transcriptional networks regulating neuronal identity in the developing spinal cord. *Nat. Neurosci.* **4 Suppl**, 1183–1191.

Lin, J., Wang, C. and Redies, C. (2012). Expression of delta-protocadherins in the spinal cord of the

chicken embryo. *J. Comp. Neurol.* **520**, 1509–1531.
Lu, D. C., Niu, T. and Alaynick, W. A. (2015). Molecular and cellular development of spinal cord locomotor circuitry. *Front. Mol. Neurosci.* **8**,.
Lutz, B., Kuratani, S., Cooney, A. J., Wawersik, S., Tsai, S. Y., Eichele, G. and Tsai, M. J. (1994). Developmental regulation of the orphan receptor COUP-TF II gene in spinal motor neurons. *Development* **120**, 25–36.
Morikawa, Y., Hisaoka, T. and Senba, E. (2009). Characterization of Foxp2-expressing cells in the developing spinal cord. *Neuroscience* **162**, 1150–1162.
Morita, K., Furuse, M., Fujimoto, K. and Tsukita, S. (1999). Claudin multigene family encoding four-transmembrane domain protein components of tight junction strands. *Proc. Natl. Acad. Sci. U. S. A.* **96**, 511–6.
Müller, T., Brohmann, H., Pierani, A., Heppenstall, P. A., Lewin, G. R., Jessell, T. M. and Birchmeier, C. (2002). The homeodomain factor Lbx1 distinguishes two major programs of neuronal differentiation in the dorsal spinal cord. *Neuron* **34**, 551–562.
Müller, T., Anlag, K., Wildner, H., Britsch, S., Treier, M. and Birchmeier, C. (2005). The bHLH factor Olig3 coordinates the specification of dorsal neurons in the spinal cord. *Genes Dev.* **19**, 733–743.
Niederreither, K., McCaffery, P., Dräger, U. C., Chambon, P. and Dollé, P. (1997). Restricted expression and retinoic acid-induced downregulation of the retinaldehyde dehydrogenase type 2 (RALDH-2) gene during mouse development. *Mech. Dev.* **62**, 67–78.
Nishi, Y., Zhang, X., Jeong, J., Peterson, K. A., Vedenko, A., Bulyk, M. L., Hide, W. A. and McMahon, A. P. (2015). A direct fate exclusion mechanism by Sonic hedgehog-regulated transcriptional repressors. *Development* **142**, 3286–93.
Novitch, B. G., Chen, A. I. and Jessell, T. M. (2001). Coordinate regulation of motor neuron subtype identity and pan-neuronal properties by the bHLH repressor Olig2. *Neuron* **31**, 773–789.
Novitch, B. G., Wichterle, H., Jessell, T. M. and Sockanathan, S. (2003). A requirement for retinoic acid-mediated transcriptional activation in ventral neural patterning and motor neuron specification. *Neuron* **40**, 81–95.
Philippidou, P. and Dasen, J. S. (2013). Hox Genes: Choreographers in Neural Development, Architects of Circuit Organization. *Neuron* **80**, 12–34.
Preibisch, S., Saalfeld, S. and Tomancak, P. (2009). Globally optimal stitching of tiled 3D microscopic image acquisitions. *Bioinformatics* **25**, 1463–1465.
Price, S. R., De Marco Garcia, N. V., Ranscht, B. and Jessell, T. M. (2002). Regulation of motor neuron pool sorting by differential expression of type II cadherins. *Cell* **109**, 205–216.
Rosenberg, A. B., Roco, C. M., Muscat, R. A., Kuchina, A., Sample, P., Yao, Z., Graybuck, L. T., Peeler, D. J., Mukherjee, S., Chen, W., et al. (2018). Single-cell profiling of the developing mouse brain and spinal cord with split-pool barcoding. *Science (80-.).* **360**, 176–182.
Rousso, D. L., Gaber, Z. B., Wellik, D., Morrisey, E. E. and Novitch, B. G. (2008). Coordinated Actions of the Forkhead Protein Foxp1 and Hox Proteins in the Columnar Organization of Spinal Motor Neurons. *Neuron* **59**, 226–240.
Roy, a., Francius, C., Rousso, D. L., Seuntjens, E., Debruyn, J., Luxenhofer, G., Huber, a. B., Huylebroeck, D., Novitch, B. G. and Clotman, F. (2012). Onecut transcription factors act upstream of Isl1 to regulate spinal motoneuron diversification. *Development* **139**, 3109–3119.
Sagner, A., Gaber, Z. B., Delile, J., Kong, J. H., Rousso, D. L., Pearson, C. A., Weicksel, S. E., Melchionda, M., Mousavy Gharavy, S. N., Briscoe, J., et al. (2018). Olig2 and Hes regulatory dynamics during motor neuron differentiation revealed by single cell transcriptomics. *PLOS Biol.* **16**, e2003127.
Sathyamurthy, A., Johnson, K. R., Matson, K. J. E., Dobrott, C. I., Li, L., Ryba, A. R., Bergman, T. B., Kelly, M. C., Kelley, M. W. and Levine, A. J. (2018). Massively Parallel Single Nucleus Transcriptional Profiling Defines Spinal Cord Neurons and Their Activity during Behavior. *Cell Rep.* **22**, 2094–2106.

Saunders, A., Macosko, E. Z., Wysoker, A., Goldman, M., Krienen, F. M., de Rivera, H., Bien, E., Baum, M., Bortolin, L., Wang, S., et al. (2018). Molecular Diversity and Specializations among the Cells of the Adult Mouse Brain. *Cell* **174**, 1015–1030.e16.

Setty, M., Tadmor, M. D., Reich-zeliger, S., Angel, O., Salame, T. M., Kathail, P., Choi, K., Bendall, S., Friedman, N. and Pe, D. (2016). Articles Wishbone identifies bifurcating developmental trajectories from single-cell data. *Nat. Biotechnol.* **34**, 614–637.

Sharma, K., Sheng, H. Z., Lettieri, K., Li, H., Karavanov, A., Potter, S., Westphal, H. and Pfaff, S. L. (1998). LIM homeodomain factors Lhx3 and Lhx4 assign subtype identities for motor neurons. *Cell* **95**, 817–828.

Shekhar, K., Lapan, S. W., Whitney, I. E., Tran, N. M., Macosko, E. Z., Kowalczyk, M., Adiconis, X., Levin, J. Z., Nemesh, J., Goldman, M., et al. (2016). Comprehensive Classification of Retinal Bipolar Neurons by Single-Cell Transcriptomics. *Cell* **166**, 1308–1323.e30.

Shin, J., Berg, D. A., Christian, K. M., Shin, J., Berg, D. A., Zhu, Y., Shin, J. Y., Song, J. and Bonaguidi, M. A. (2015). Single-Cell RNA-Seq with Waterfall Reveals Molecular Cascades underlying Adult Neurogenesis Resource Single-Cell RNA-Seq with Waterfall Reveals Molecular Cascades underlying Adult Neurogenesis. *Stem Cell* **17**, 360–372.

Sockanathan, S. and Jessell, T. M. (1998). Motor Neuron–Derived Retinoid Signaling Specifies the Subtype Identity of Spinal Motor Neurons. *Cell* **94**, 503–514.

Sommer, L., Ma, Q. and Anderson, D. J. (1996). neurogenins, a novel family of atonal-related bHLH transcription factors, are putative mammalian neuronal determination genes that reveal progenitor cell heterogeneity in the developing CNS and PNS. *Mol. Cell. Neurosci.* **8**, 221–241.

Stam, F. J., Hendricks, T. J., Zhang, J., Geiman, E. J., Francius, C., Labosky, P. A., Clotman, F. and Goulding, M. (2012). Renshaw cell interneuron specialization is controlled by a temporally restricted transcription factor program. *Development* **139**, 179–190.

Stifani, N. (2014). Motor neurons and the generation of spinal motor neuron diversity. *Front. Cell. Neurosci.* **8**, 293.

Stolt, C. C., Lommes, P., Sock, E., Chaboissier, M. C., Schedl, A. and Wegner, M. (2003). The Sox9 transcription factor determines glial fate choice in the developing spinal cord. *Genes Dev.* **17**, 1677–1689.

Südhof, T. C. (2017). Synaptic Neurexin Complexes: A Molecular Code for the Logic of Neural Circuits. *Cell* **171**, 745–769.

Sweeney, L. B., Bikoff, J. B., Gabitto, M. I., Brenner-Morton, S., Baek, M., Yang, J. H., Tabak, E. G., Dasen, J. S., Kintner, C. R. and Jessell, T. M. (2018). Origin and Segmental Diversity of Spinal Inhibitory Interneurons. *Neuron* 1–15.

Tanay, A. and Regev, A. (2017). Scaling single-cell genomics from phenomenology to mechanism. *Nature* **541**, 331–338.

Trapnell, C., Cacchiarelli, D., Grimsby, J., Pokharel, P., Li, S., Morse, M., Lennon, N. J., Livak, K. J., Mikkelsen, T. S. and Rinn, J. L. (2014). The dynamics and regulators of cell fate decisions are revealed by pseudotemporal ordering of single cells. *Nat. Biotechnol.* **32**, 381–386.

Tripodi, M., Stepien, A. E. and Arber, S. (2011). Motor antagonism exposed by spatial segregation and timing of neurogenesis. *Nature* **479**, 61–66.

Uemura, T., Lee, S. J., Yasumura, M., Takeuchi, T., Yoshida, T., Ra, M., Taguchi, R., Sakimura, K. and Mishina, M. (2010). Trans-synaptic interaction of GluRδ2 and neurexin through Cbln1 mediates synapse formation in the cerebellum. *Cell* **141**, 1068–1079.

Wagner, A., Regev, A. and Yosef, N. (2016). Revealing the vectors of cellular identity with single-cell genomics. *Nat. Biotechnol.* **34**, 1145–1160.

Zeisel, A., Hochgerner, H., Lönnerberg, P., Johnsson, A., Memic, F., van der Zwan, J., Häring, M., Braun, E., Borm, L. E., La Manno, G., et al. (2018). Molecular Architecture of the Mouse Nervous System. *Cell* **174**, 999–1014.e22.

Figures

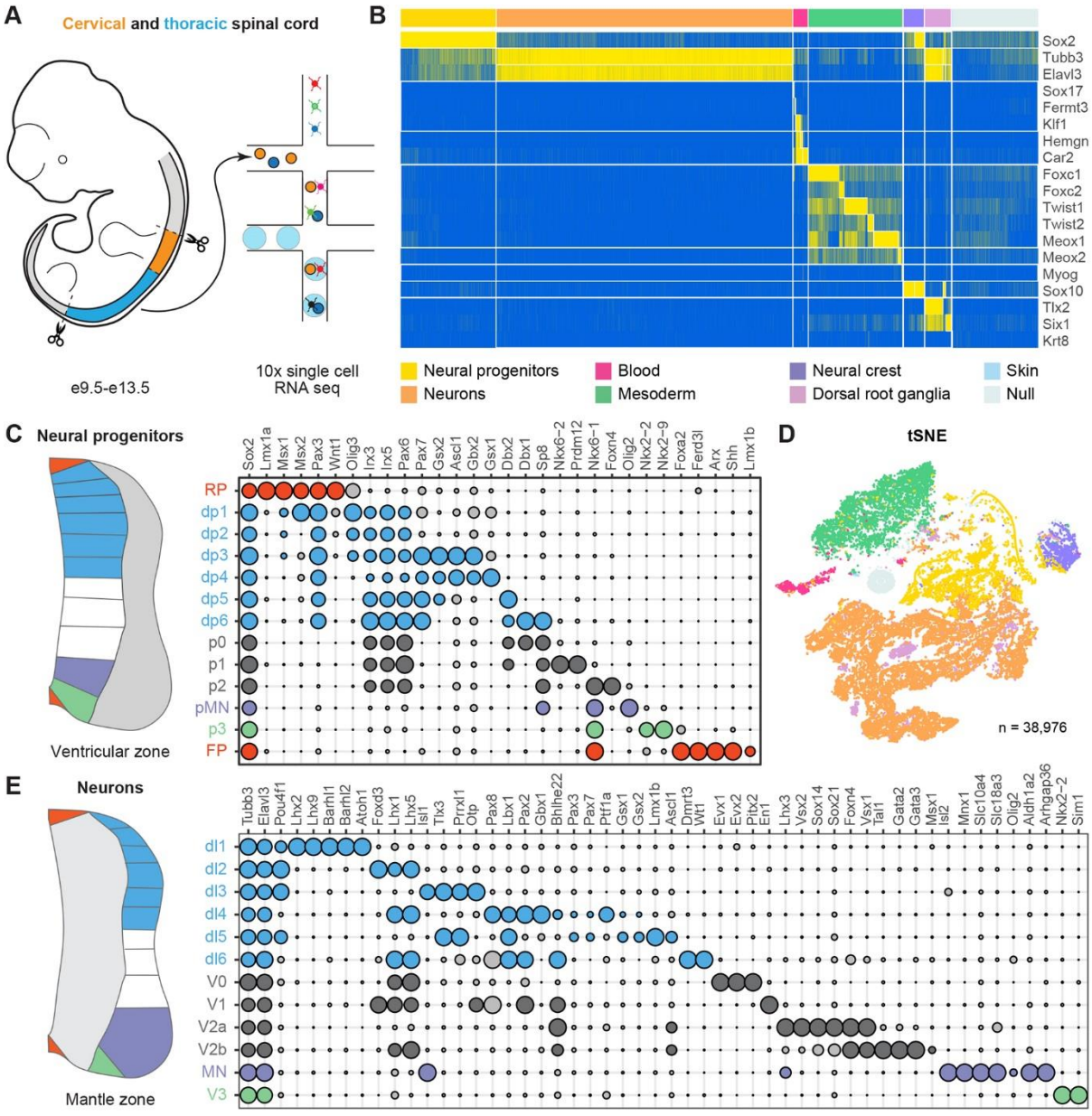

Figure 1: High throughput scRNA-seq from the developing spinal cord.

(A) Cervical (orange) and thoracic (blue) regions of the spinal cord of mouse embryos between stage e9.5 to e13.5 were dissected, dissociated and sequenced using the Chromium 10x Genomics system.

(B) Partitioning of cells to specific tissue types based on the combinatorial expression of known markers.

(C,E) Bubble charts depicting the expression of markers used to identify dorsal-ventral domains of progenitors (C) and neuronal classes (E). Circle size indicates normalized gene expression levels. Genes

selected for cell categorisation are coloured; grey circles correspond to markers not used for the selection of a specific population.
(D) t-distributed Stochastic Neighbor Embedding (tSNE) plot of the entire dataset based on transcriptional similarity using the same markers as (B), coloured by assigned cell type. Neural progenitors (yellow) and neurons (orange) were selected for further analysis.

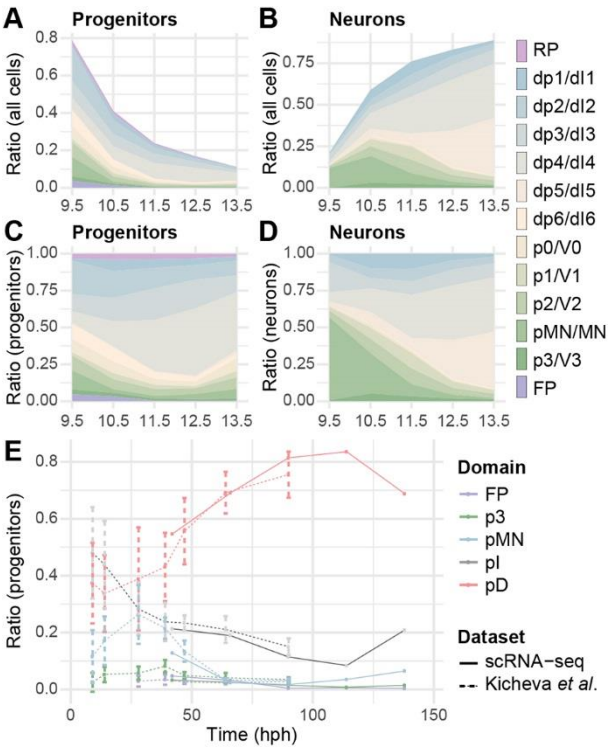

Figure 2: Dynamics of domain sizes based on the single cell sequencing data.

(A-D) Changes in the fraction of progenitors (A,C) and neurons (B,D) between e9.5 and e13.5. (A,B) The data are normalised to the sum of neurons and progenitors detected at each time point. (C,D) show fractions within progenitors (B) or neurons (D).

(E) Comparison of the ratio of progenitors from our dataset (solid lines) with those of Kicheva et al. (2014; dashed lines). The broader domains pI and pD are composed of p0-p2 and pd1-pd6 progenitors, respectively.

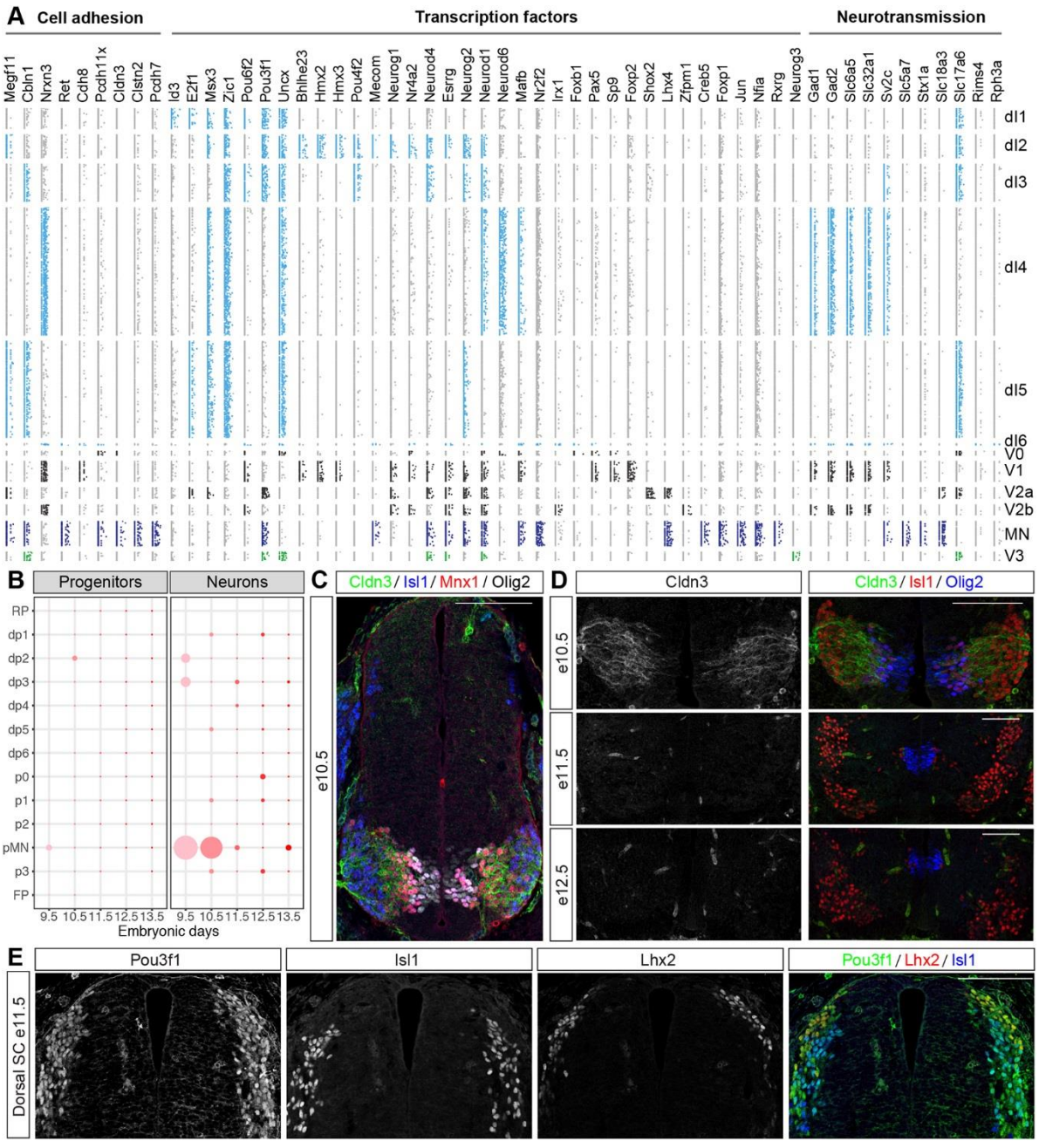

Figure 3: Spatial and temporal patterns of gene expression in neural progenitors and neurons.

(A) Identification of differentially expressed genes encoding cell adhesion molecules, TFs and proteins involved in neurotransmission. Genes used in the initial partitioning of cell types are not shown.

(B) Spatial and temporal expression of Cldn3 in neural progenitors and neurons in the dataset. Cldn3 is specifically expressed in MNs until e10.5.

(C) Immunostaining at e10.5 for Cldn3 (green), Isl1 (blue), Mnx1 (red) and Olig2 (grey).

(D) Cldn3 expression is specific to MNs at e10.5, and lost in MNs at e11.5 and e12.5.

(E) Pou3f1 is expressed in dorsal d1-3 neurons at e11.5. dI1 neurons are labelled by Lhx2, and dI3 neurons by Isl1 expression.

Scale bars = 100 µm

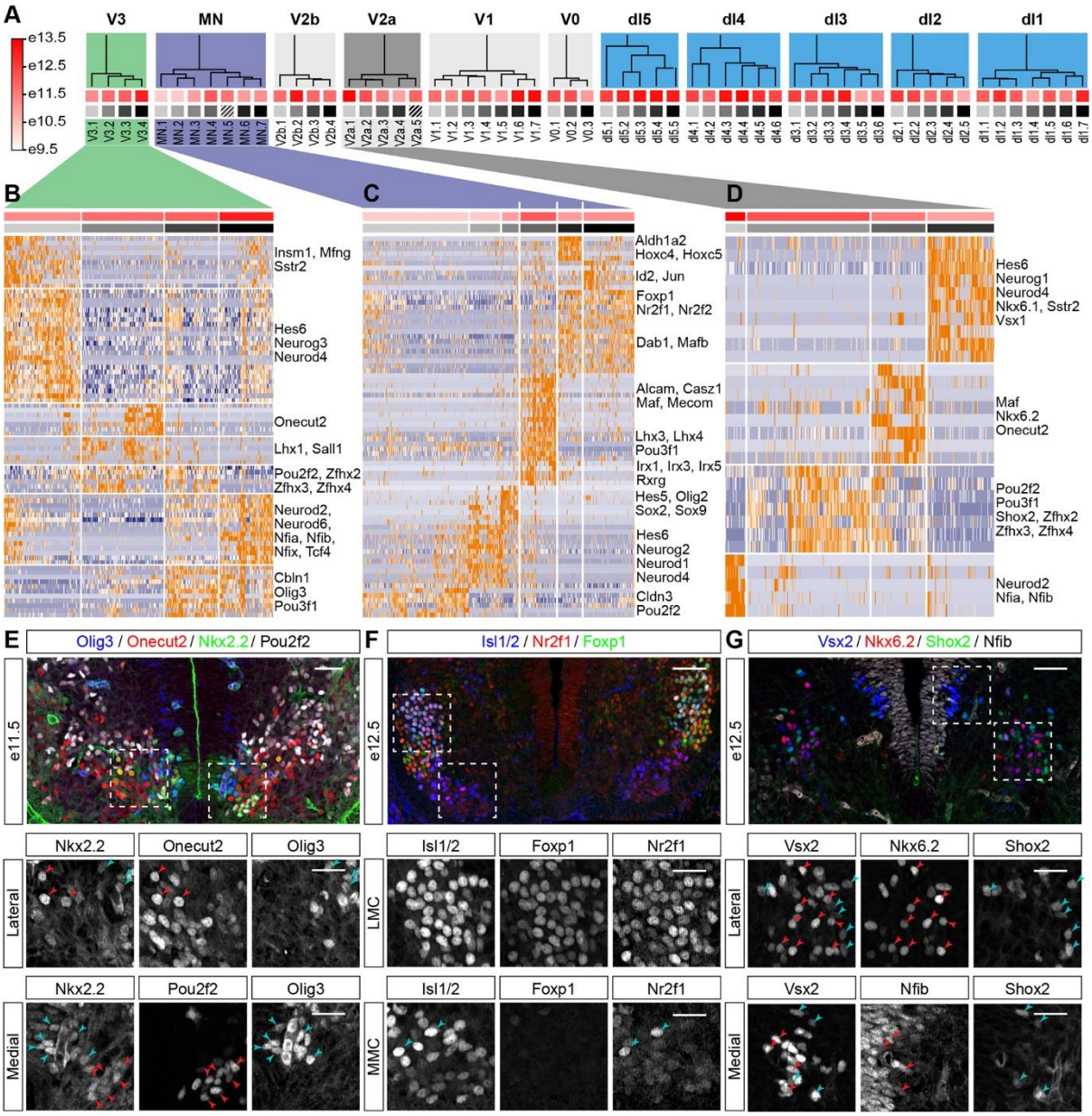

Figure 4: Hierarchical clustering identifies neuronal subtypes and implicates TFs in determining their identity.

(A) Hierarchical clustering of the cardinal types of spinal cord neurons reveals 59 neuronal subtypes. Dendrograms for each neuronal domain are depicted. Squares under the dendrogram indicate average age (red squares) and neuronal subtype identity (grey squares). Colours of squares correspond to those shown on top of the heatmaps in Fig 4B-D and Fig S4. Striped squares correspond to incorrectly classified cells that were discarded from further analysis.

(B-D) Identification of neuronal subtypes by clustering of gene expression profiles in V3 (B), MNs (C) and V2a interneurons (D). Hierarchical clustering was performed using the indicated gene modules (Table S2). A subset of genes included in the modules is indicated on the righthand side.

(E-G) Validation of predicted gene expression patterns obtained from the hierarchical clustering in (B-D). (E) Expression of Pou2f2 is detected in Nkx2.2-expressing V3 neurons at e11.5. Pou2f2 expression does not overlap with Onecut2 in more dorsal V3 neurons (top row) or Olig3 in V3 neurons abutting the p3 domain (bottom row). (F) Nr2f1 expression in Foxp1+ LMC neurons at e12.5 (top row). A few Nr2f1-positive cells are also detected in Foxp1-negative MNs within the MMC (bottom row). (G) Nkx6.2 expression in lateral Vsx2-expressing V2a neurons does not overlap Shox2 expression at e12.5 (top row). Nfib expression is confined to medial V2a neurons at this stage (bottom row).
Scale bars = 50 µm, scale bars of insets are 25 µm

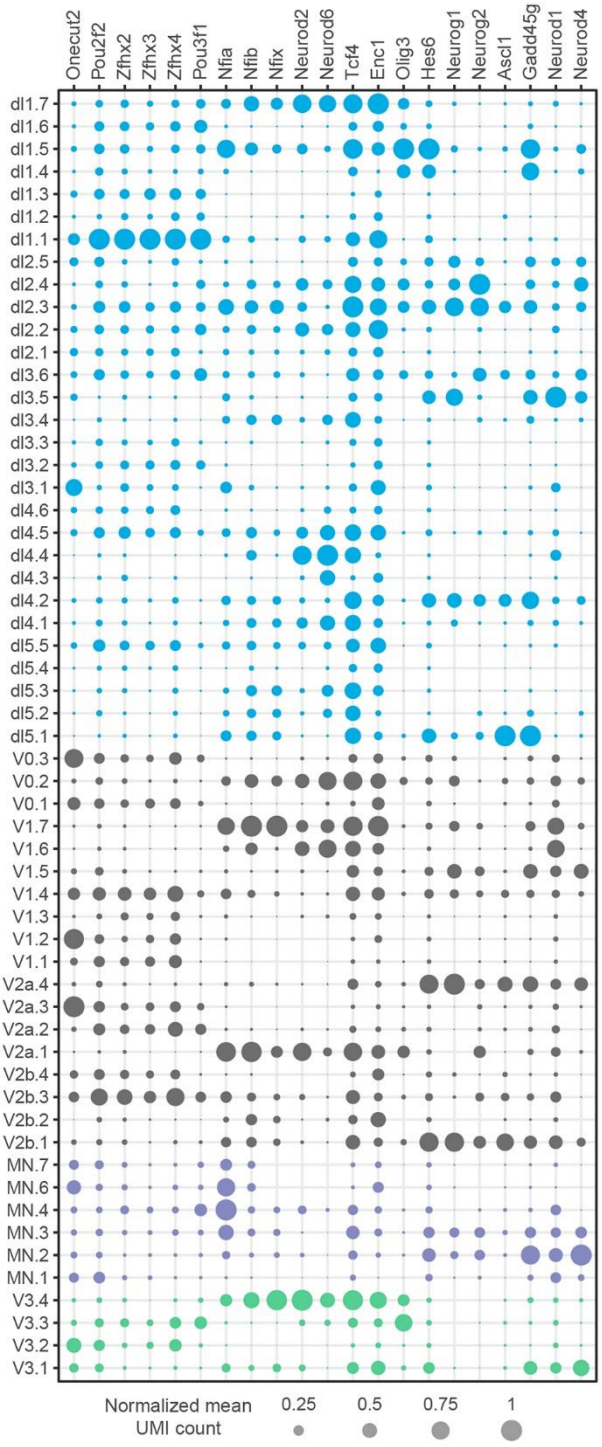

Figure 5: Subdivision of neuronal classes by a shared set of TFs

Gene expression profiles of TFs that define subpopulations of neurons in multiple domains. Circle size indicates normalized gene expression levels.

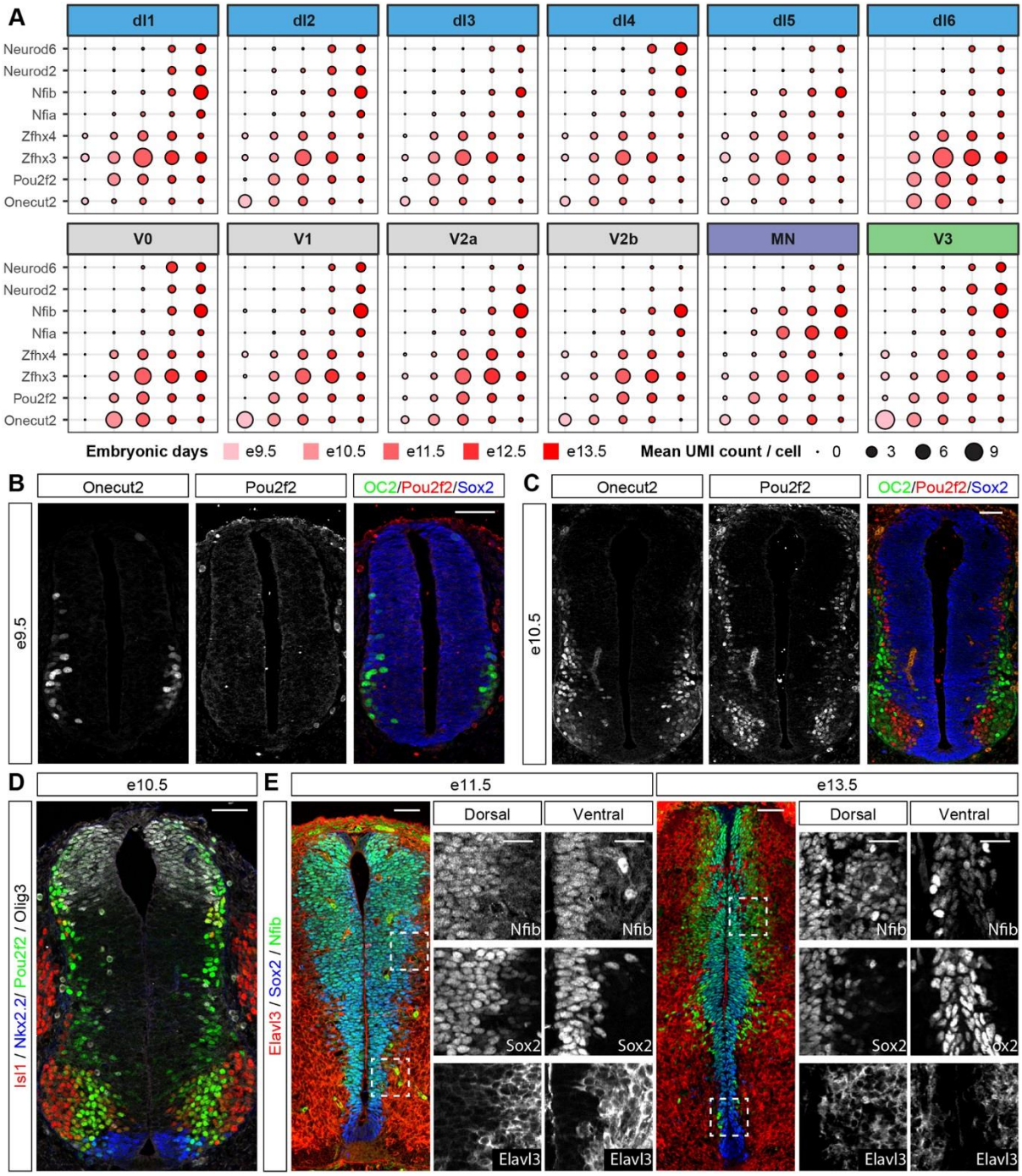

Figure 6: Temporal stratification of neuronal subtypes by shared sets of TFs.

(A) Temporal expression of a shared set of TFs in different neuronal populations identifies two waves of neurogenesis. The size of the circles indicates the mean expression of genes per stage and domain.

(B) Onecut2, but not Pou2f2, is expressed in neurons at e9.5.

(C) Mutually exclusive expression of Onecut2 and Pou2f2 in spinal cord neurons at e10.5. Note that Onecut2 expressing neurons are typically located more laterally than Pou2f2^{+} neurons.

(D) Widespread expression of Pou2f2 at e10.5 in differentiating neurons close to the ventricular zone. Pou2f2 expression colocalizes with Olig3, Nkx2.2 and Isl1.

(E) Increased expression of Nfib in differentiating neurons at late developmental stages. Nfib is expressed at low levels at e11.5 in progenitors labelled with Sox2 and is not detected in neurons. By contrast, at e13.5 Nfib expression is observed in neurons that also express the neuronal marker Elavl3. Scale bars = 50 µm, scale bars of insets are 25 µm

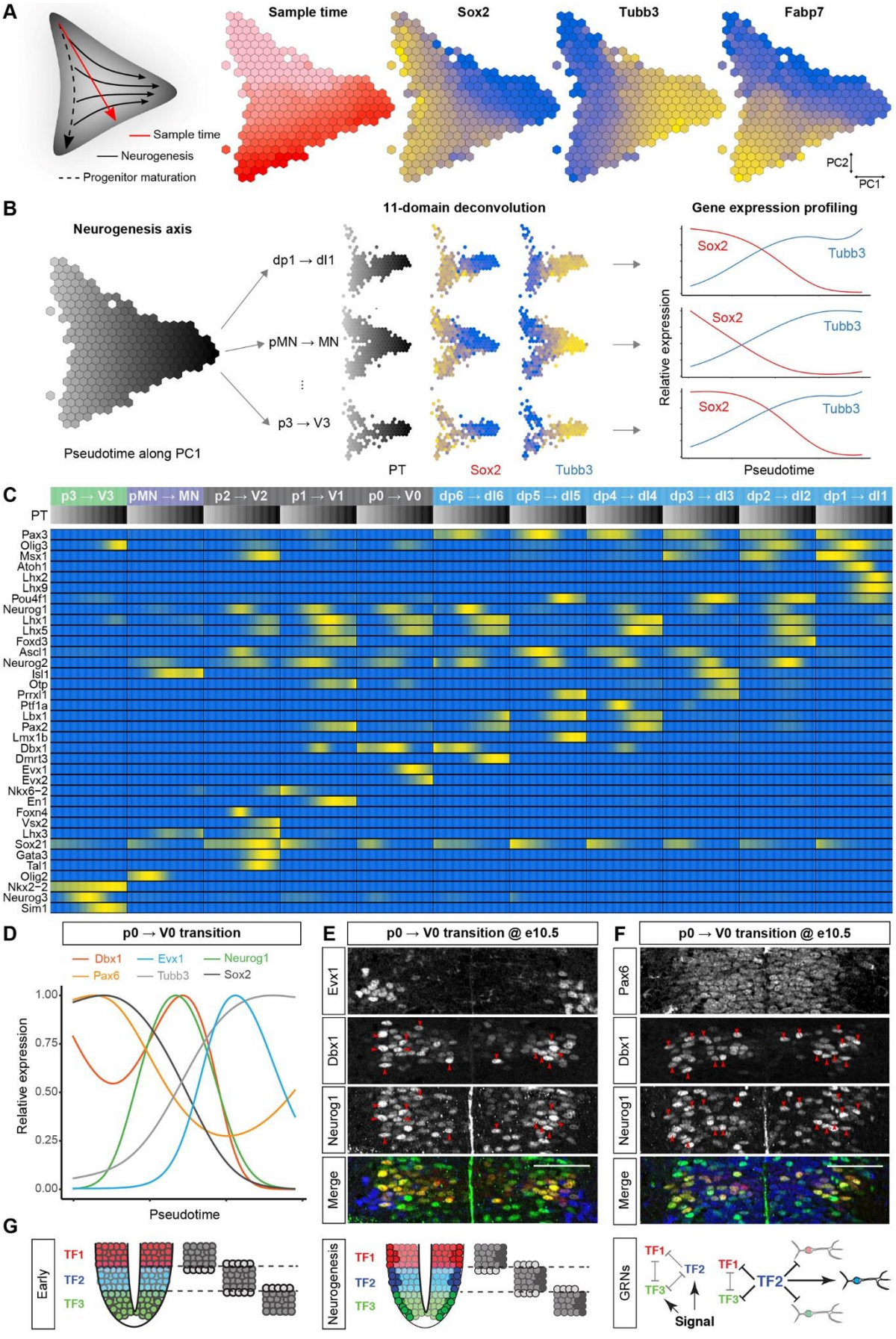

Figure 7: Pseudotemporal ordering reveals gene expression dynamics during neurogenesis
(A) PCA projection of all neural cells, shown on a hexagonal heatmap, from a 100-dimensional space defined by genes expressed in all dorsal-ventral domains during progenitor maturation and neurogenesis. The graph on the left depicts from top to bottom progenitor maturation, while the arrows from left to right mark neurogenesis. The hexagonal heatmaps indicate the number of cells from different developmental stages, and the expression pattern of the pan-progenitor marker Sox2, the neuronal marker Tubb3, and the gliogenic marker Fabp7.
(B) The first principal component of the cell state graph was used to independently reconstruct neurogenesis in each dorsal-ventral domain. Cells allocated to specific DV domains were plotted along the differentiation trajectory, and the expression profile of genes independently reconstructed.
(C) Upregulation of domain specific TFs coincides with neurogenesis in multiple domains. Heatmap including the normalized expression pattern (low blue, high yellow) of genes involved in neurogenesis per domain along the pseudotemporal axis (grey early, black late).
(D) Smoothed expression profile of the neurogenic trajectory from p0 to V0 shows a transient upregulation of Dbx1 prior to neurogenesis that coincides with the maximal expression of Neurog1.
(E-F) Upregulation of Dbx1 coincides with Neurog1 expression. (E) Co-expression of Dbx1 and Neurog1 in cells in the differentiation zone of the ventricular layer in the p0 domain at eE10.5. V0 neurons are identified by the expression of Evx1. (F) While Dbx1 expression is maximal in differentiating progenitors at e10.5, Pax6 expression is homogeneous in all p0 progenitors.
(G) Domain-specific TFs are upregulated prior to neurogenesis. Initially, domain-specific TFs specify progenitor identity. Upon neurogenesis, domain specific TF expression is transiently upregulated to reinforce the subtype identity of the differentiating neurons.
Scale bars = 50 μm

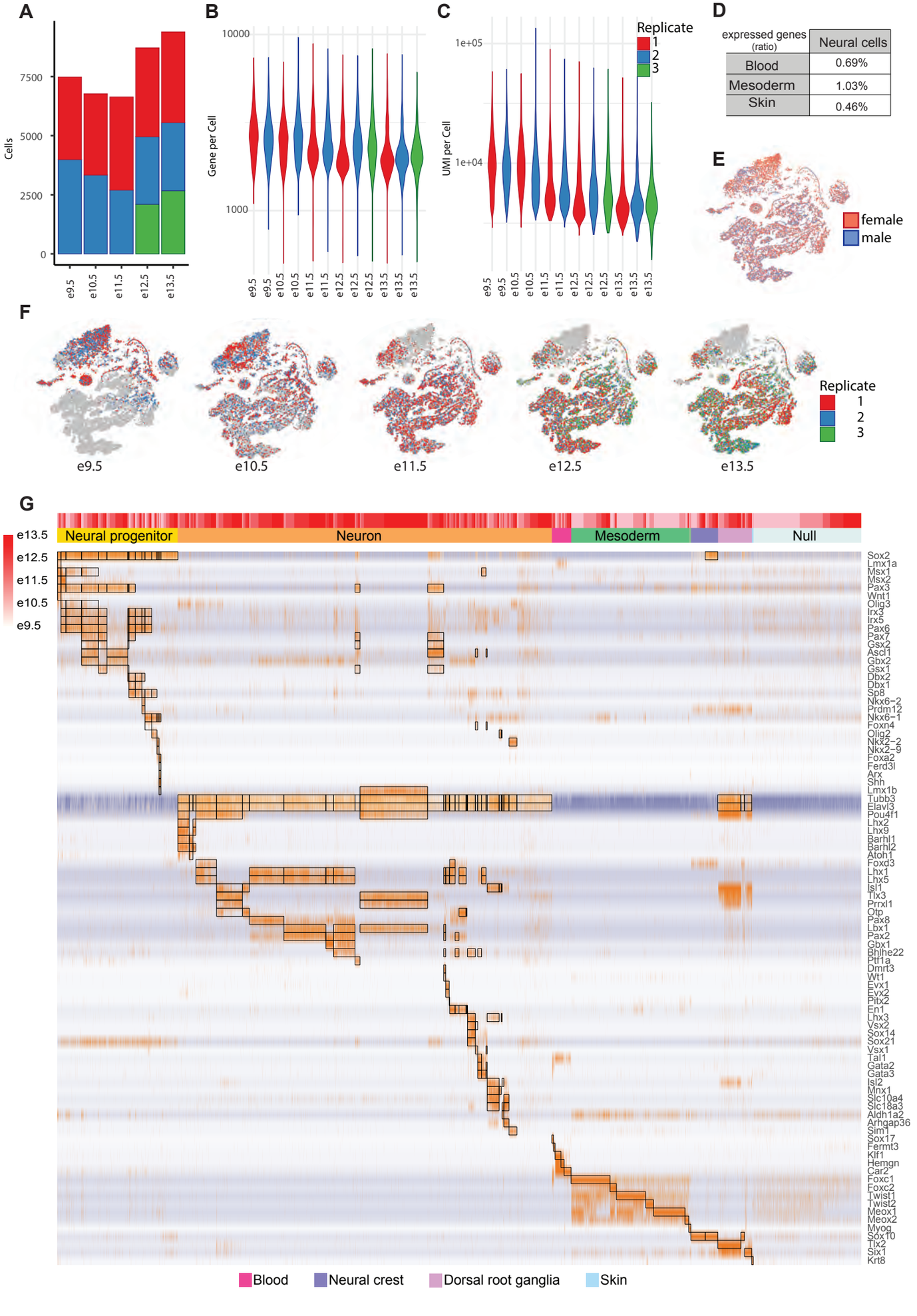
A
Cells
7500
5000
2500
0
e9.5
e10.5
e11.5
e12.5
e13.5
B
Gene per Cell
10000
1000
C
UMI per Cell
1e+05
1e+04
Replicate
1
2
3
D
expressed genes (ratio)
Neural cells
Blood 0.69%
Mesoderm 1.03%
Skin 0.46%
E
female
male
F
e9.5
e10.5
e11.5
e12.5
e13.5
Replicate
1
2
3
G
e13.5
e12.5
e11.5
e10.5
e9.5
Neural progenitor
Neuron
Mesoderm
Null
Sox2
Lmx1a
Msx1
Msx2
Pax3
Wnt1
Olig3
Irx3
Irx5
Pax6
Pax7
Gsx2
Ascl1
Gbx2
Gsx1
Dbx2
Dbx1
Sp8
Nkx6-2
Prdm12
Nkx6-1
Foxn4
Olig2
Nkx2-2
Nkx2-9
Foxa2
Ferd3l
Arx
Shh
Lmx1b
Tubb3
Elavl3
Pou4f1
Lhx2
Lhx9
Barhl1
Barhl2
Atoh1
Foxd3
Lhx1
Lhx5
Isl1
Tlx3
Prrxl1
Otp
Pax8
Lbx1
Pax2
Gbx1
Bhlhe22
Ptf1a
Dmrt3
Wt1
Evx1
Evx2
Pitx2
En1
Lhx3
Vsx2
Sox14
Sox21
Vsx1
Tal1
Gata2
Gata3
Isl2
Mnx1
Slc10a4
Slc18a3
Aldh1a2
Arhgap36
Sim1
Sox17
Fermt3
Klf1
Hemgn
Car2
Foxc1
Foxc2
Twist1
Twist2
Meox1
Meox2
Myog
Sox10
Tlx2
Six1
Krt8
Blood
Neural crest
Dorsal root ganglia
Skin

Figure S1: Further characterization of the single cell transcriptome dataset.
(A) Number of cells per replicate and timepoint.
(B) Number of genes per cell for each replicate.
(C) Number of unique molecular identifiers (UMIs) per cell for each replicate.
(D) Ratio of blood (Sox17, Fermt3, Klf1, Hemgn, Car2), mesoderm (Foxc1, Foxc2, Twist1, Twist2, Meox1, Meox2) and skin (Krt8) markers expressed in neural cells.
(E,F) tSNE-plots showing the distribution of male and female cells in the dataset (E), and the different replicates per timepoint (F).
(G) Heatmap showing read distributions of the genes used to assign cell identities to the single cell transcriptomic profiles. Boxed regions indicate the cell identities in which the respective gene is expected to be expressed. Bars at the top of the heatmap indicate sample age (grey early, late red), and cell identity as color coded in Fig 1.

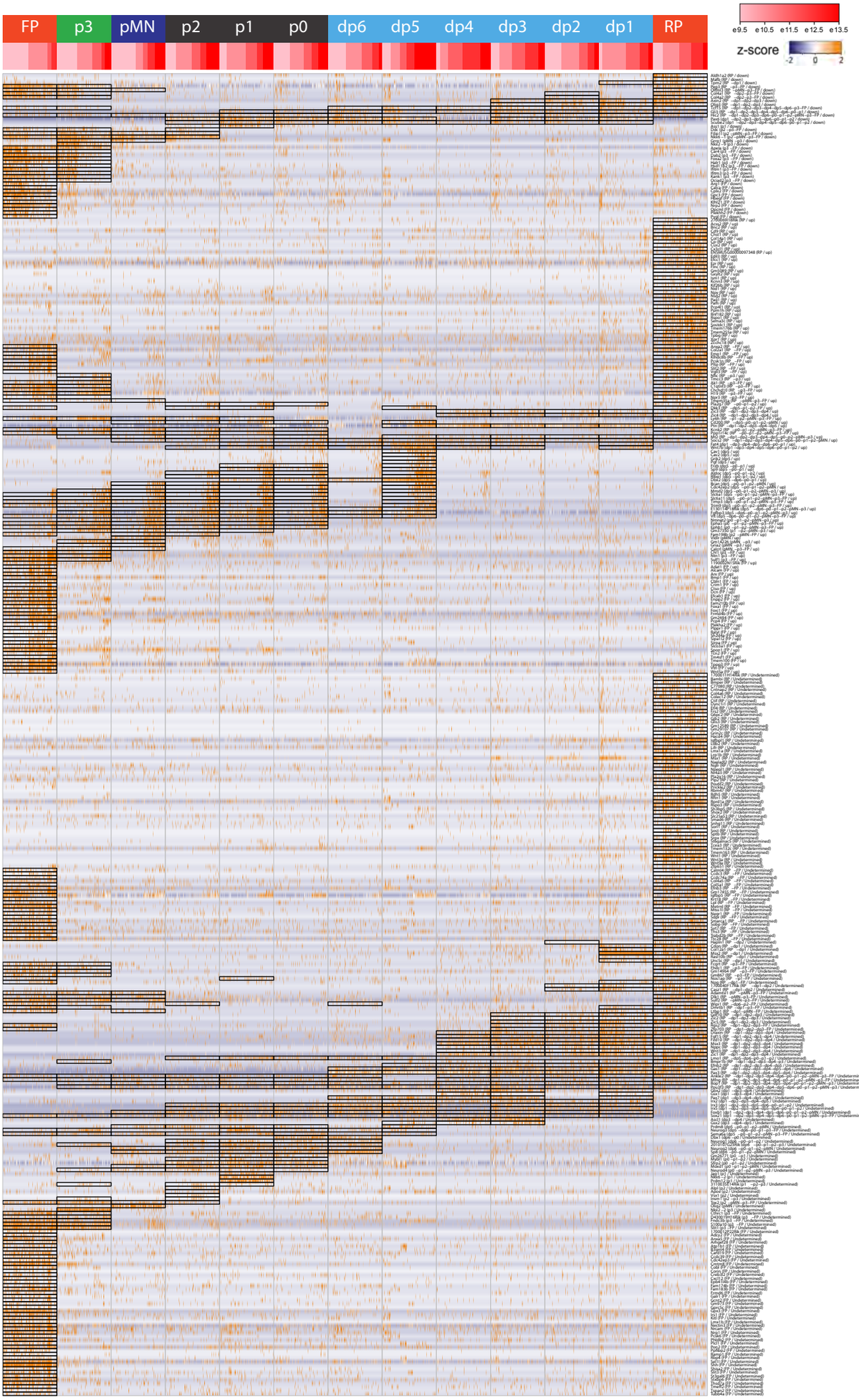
FP
p3
pMN
p2
p1
p0
dp6
dp5
dp4
dp3
dp2
dp1
RP
e9.5
e10.5
e11.5
e12.5
e13.5
z-score
-2
0
2

Figure S2: Differentially expressed genes between the different neural progenitor domains.
Heatmap showing z-scored UMI count distributions of the genes identified as differentially expressed. Domains predicted to express a gene are indicated by boxes. Cells within each domain are ordered by sample time. Rows are ordered according to the correlation between gene expression and sample time (first downregulated genes, $r < -.2$, then upregulated genes, $r > .2$, and finally undetermined trends).
.

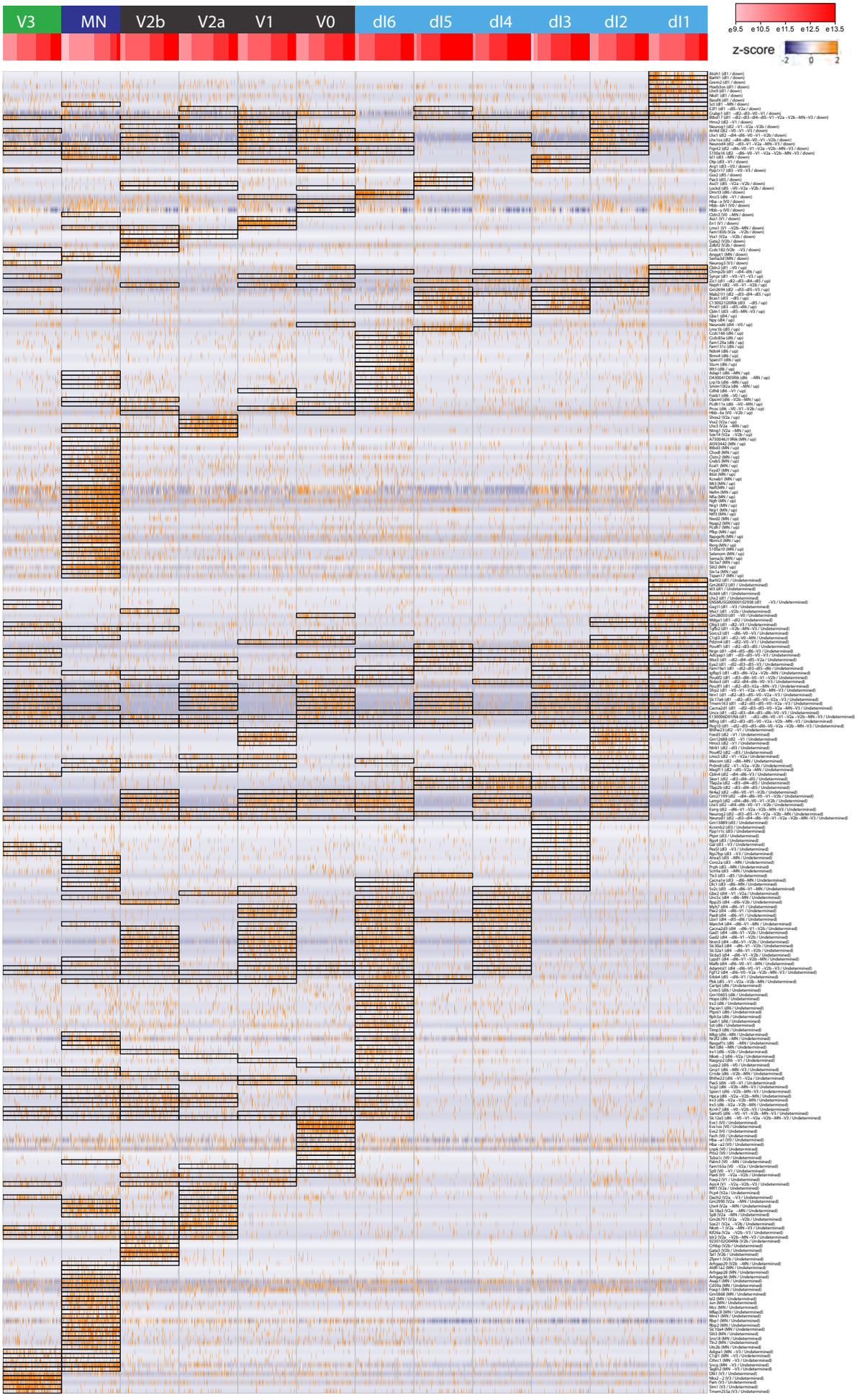
V3
MN
V2b
V2a
V1
V0
dI6
dI5
dI4
dI3
dI2
dI1
e9.5
e10.5
e11.5
e12.5
e13.5
z-score
-2
0
2

Figure S3: Differentially expressed genes between the different neuronal domains.
Heatmap showing z-scored UMI count distributions of the genes identified as differentially expressed. Domains predicted to express a gene are indicated by boxes. Cells within each domain are ordered by sample time. Rows are ordered according to the correlation between gene expression and sample time (first downregulated genes, $r < -.2$, then upregulated genes, $r > .2$, and finally indeterminant trends).

.

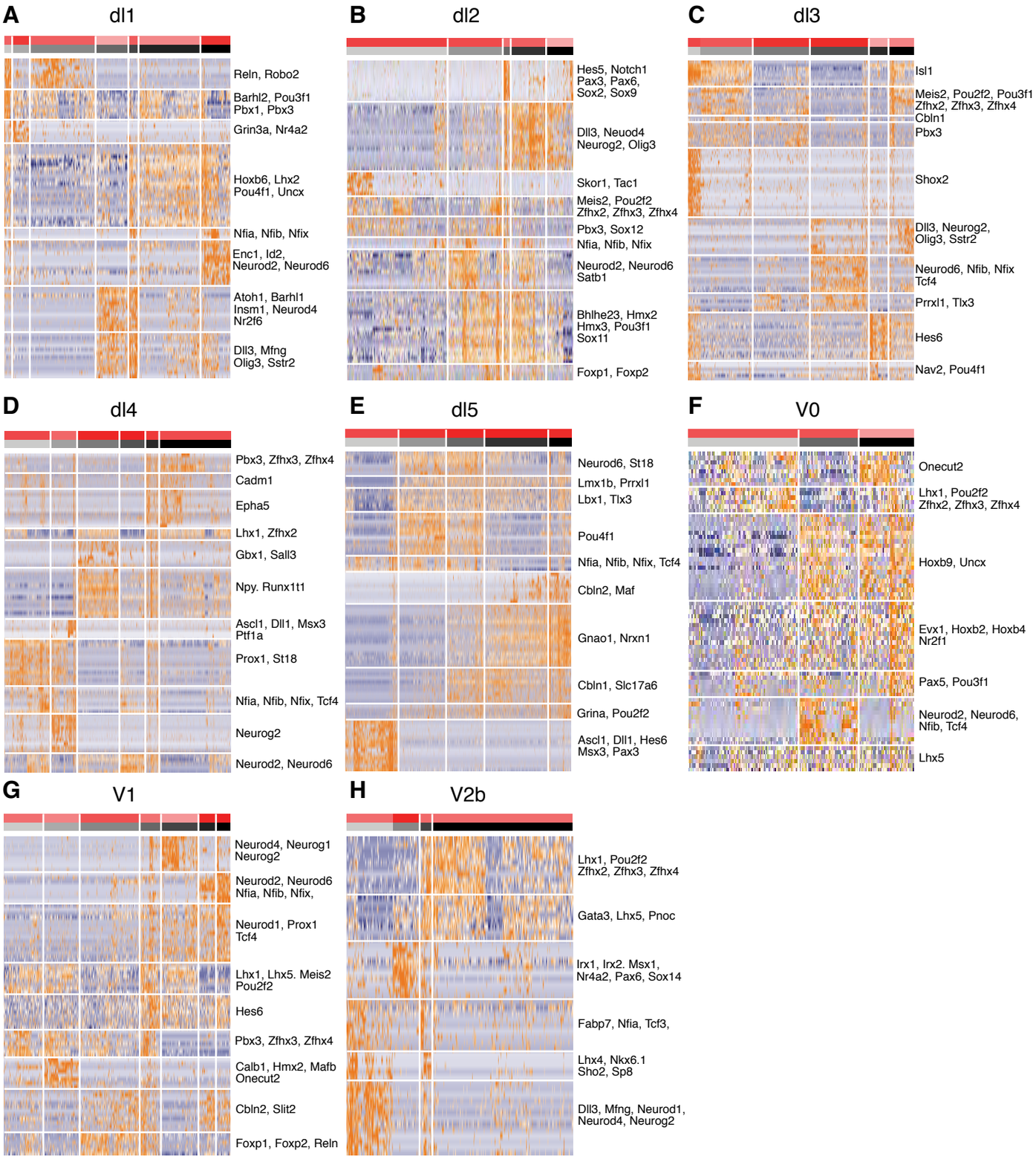

Figure S4: Hierarchical clustering of dI1, dI2, dI3, dI4, dI5, V0, V1 and V2b neurons.
Characterization of neuronal subtypes by hierarchical clustering of the indicated domains. Hierarchical clustering was performed using the curated gene modules available in Table S2. A subset of genes included in the modules are indicated on the righthand side.

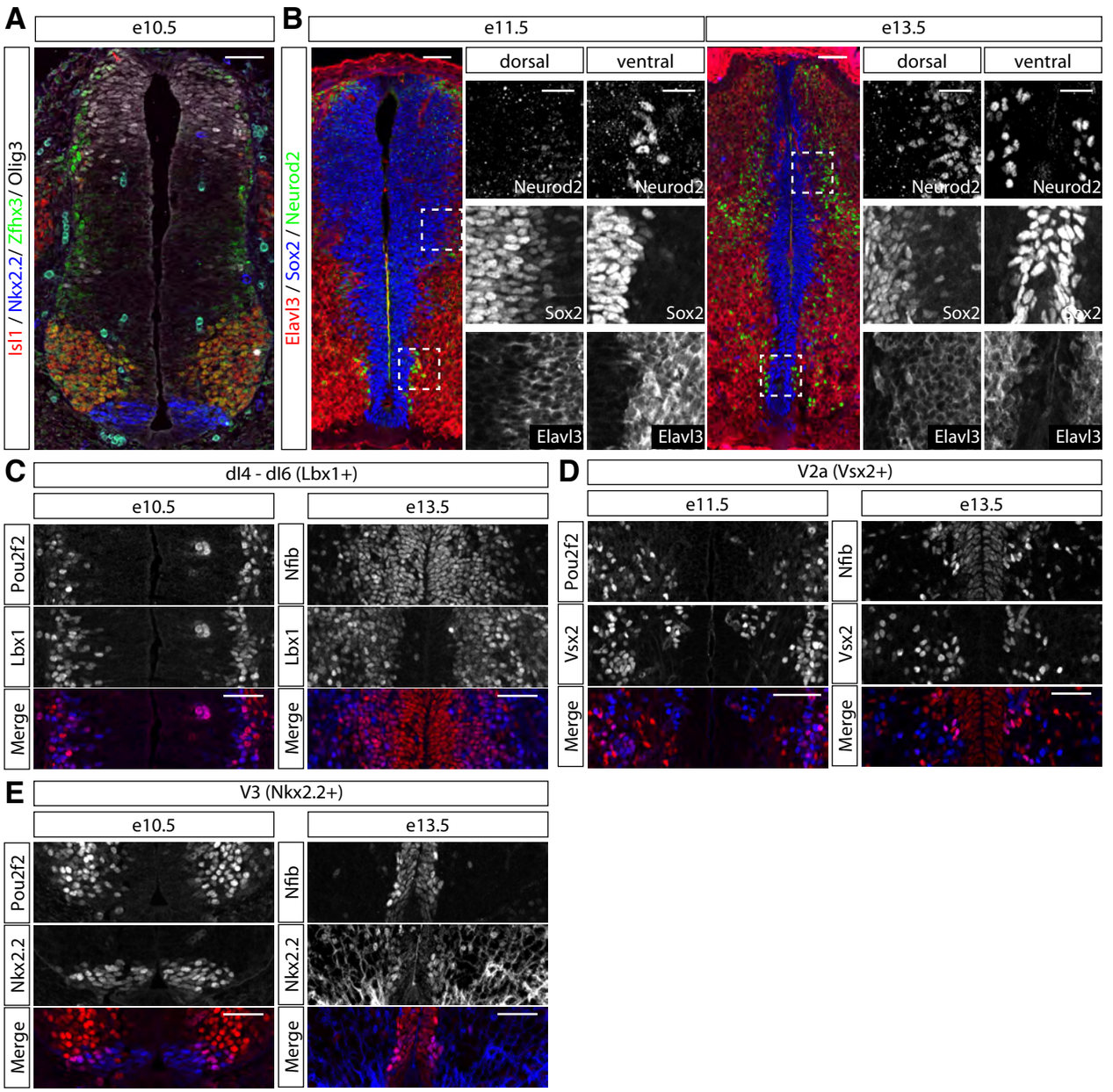

Figure S5: Temporal stratification of neuronal subtypes by a shared set of TFs

(A) Expression of Zfhx3 in neurons at e10.5

(B) Increased expression of Neurod2 in neurons after e11.5. At e11.5 only few neurons in the very dorsal and ventral spinal cord express Neurod2. Number of Neurod2 positive neurons strongly increases between e11.5 and e13.5.

(C-E) Coexpression of Pou2f2 with specific markers for multiple domains at early developmental stages (e10.5 for Nkx2.2 and Lbx1, e11.5 for Vsx2). At e13.5, Nfib is expressed in the same domains in a subset of neurons. These neurons are typically adjacent to the ventricular zone, consistent with their late birth date.

Scale bars = 50 μm, scale bars of insets are 25 μm

.

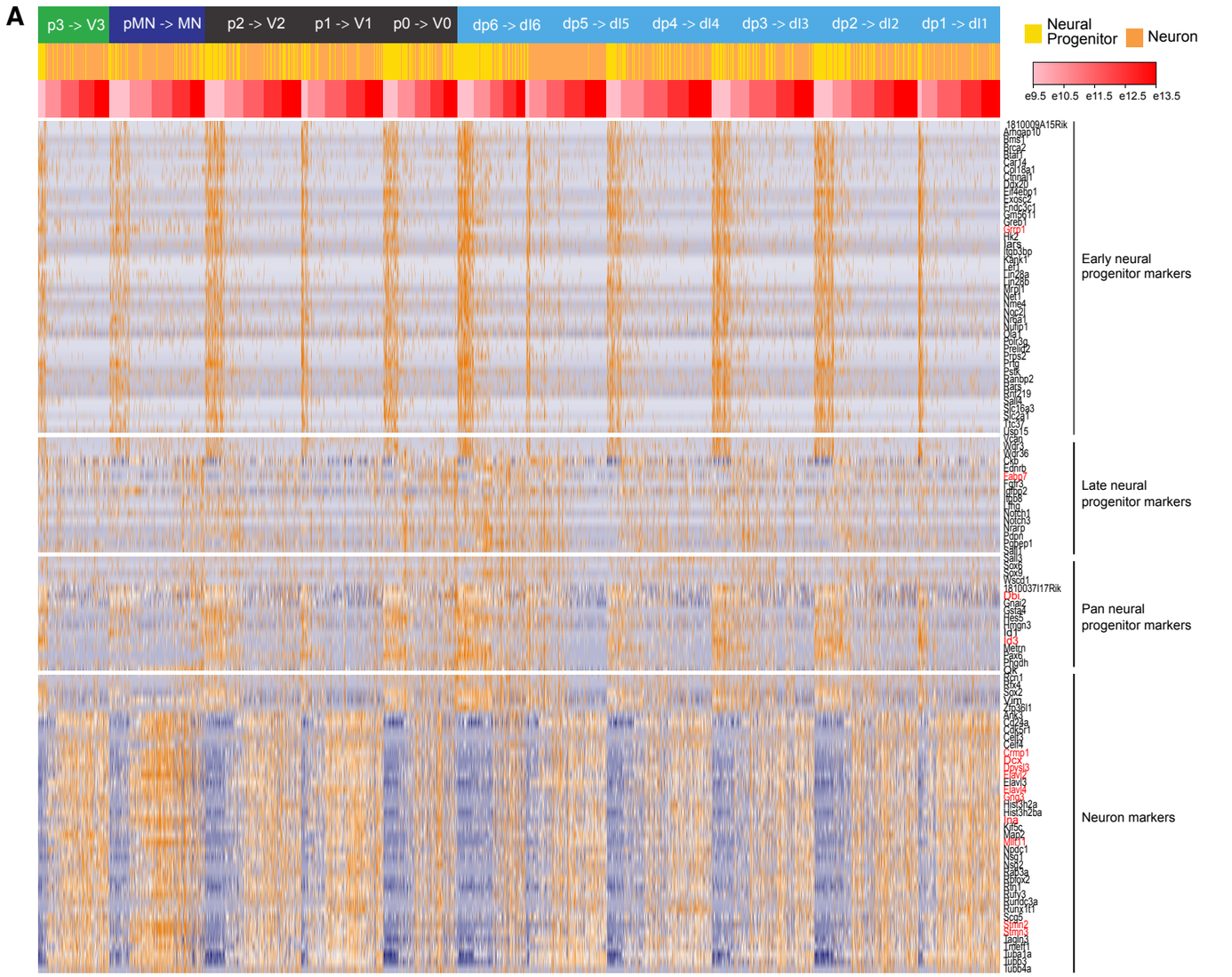

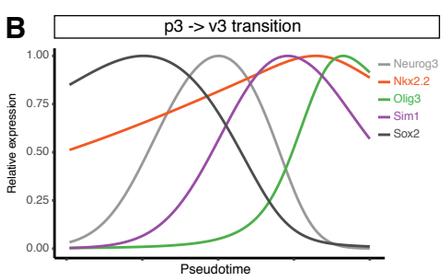

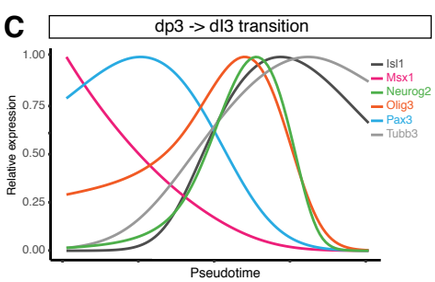

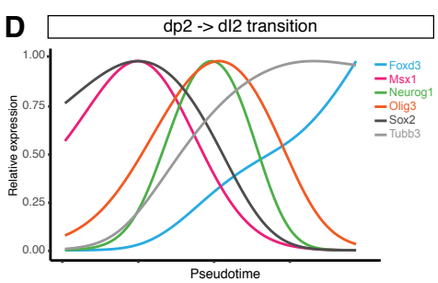

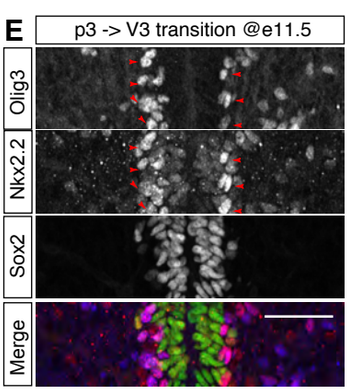

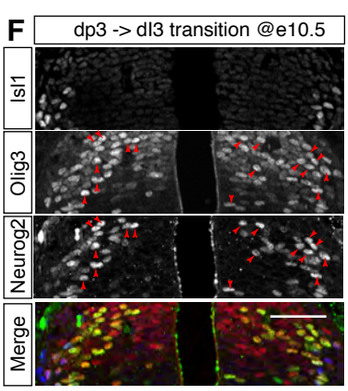

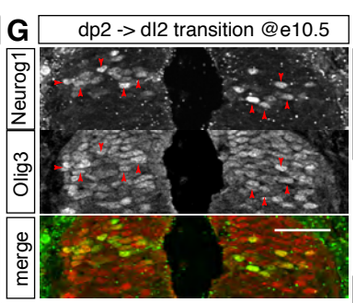

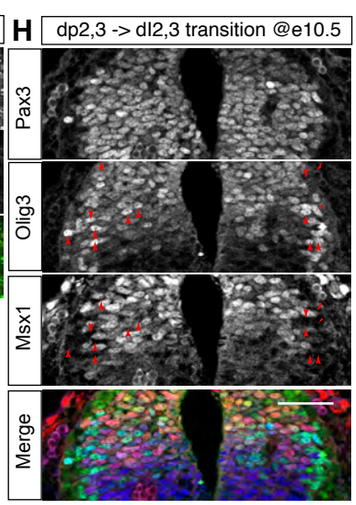

Figure S6: Pseudotime analysis reveals gene expression dynamics underlying neurogenesis in several domains.

(A) Heatmap showing the 4 genes modules identified as similarly expressed in all dorsal-ventral domains and involved in neurogenesis and progenitor maturation. Among the 114 genes, red gene labels indicate genes excluded from the following analysis because of significant dorsal-ventral bias.
(B) Smoothed expression profile of the neurogenic trajectory from p3 to V3 shows increasing levels of Nkx2.2 during neurogenesis. Note that Nkx2.2 in contrast to other neural progenitor markers continues to be expressed in V3 neurons.
(C) Smoothed expression profile of the neurogenic trajectory from dp3 to dI3 shows a transient upregulation of Olig3 prior to neurogenesis that coincides with the maximal expression of Neurog2.
(D) Smoothed expression profile of the neurogenic trajectory from dp2 to dI2 shows a transient upregulation of Olig3 prior to neurogenesis that coincides with the maximal expression of Neurog1.
(E) Upregulation of Nkx2.2 in Olig3+ (red arrows) V3 neurons compared to Sox2+ Nkx2.2 p3 progenitors at e11.5.
(F) Upregulation of Olig3 in neurogenic dp3 progenitors labelled by Neurog2 (red arrows).
(G) Upregulation of Olig3 in neurogenic dp2 progenitors labelled by Neurog1 (red arrows).
(H) Specific upregulation of Olig3 is anti-correlated with Msx1 (red arrows). The broadly dorsal progenitor marker Pax3 is homogeneously expressed in dp2 and dp3 domains.
Scale bars = 50 μm

SUPPLEMENTAL TABLES

Table S1. Knowledge matrix used to identify cell types. Columns indicate the cell type classes and rows the genes. A gene contributes to a class definition if the associated value is 1.

Click here to Download Table S1

Table S2. Curated gene lists used to cluster the neuronal subtypes in each dorsal-ventral domain.

Click here to Download Table S2

Table S3. List of primary antibodies including manufacturer and the dilutions used.

Click here to Download Table S3

Table S4. Summary table indicating the number of genes and modules for each step of the gene module identification method used to cluster the neuronal subtypes.

Click here to Download Table S4

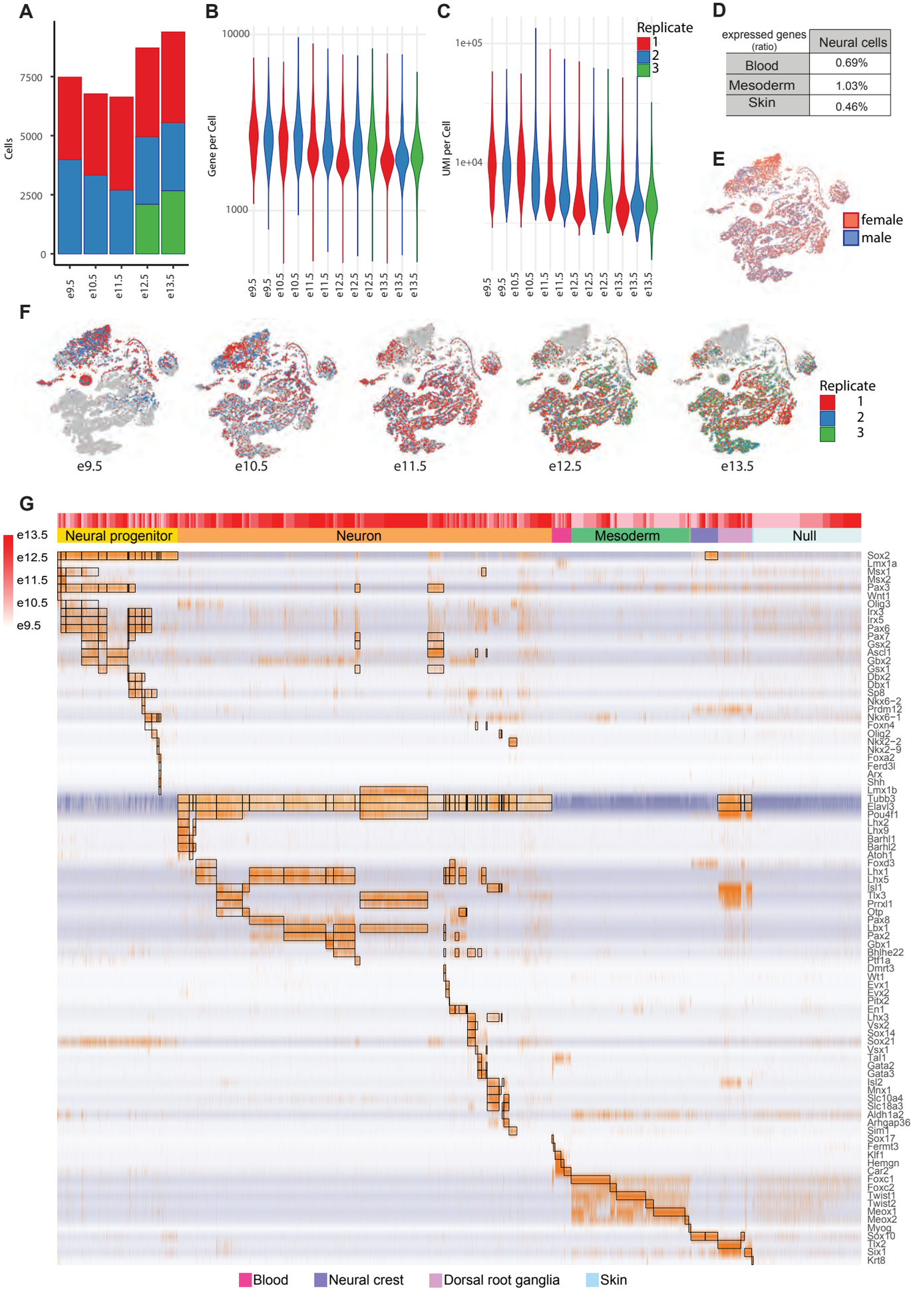
A
Cells
7500
5000
2500
0
e9.5
e10.5
e11.5
e12.5
e13.5
B
Gene per Cell
10000
1000
C
UMI per Cell
1e+05
1e+04
Replicate
1
2
3
D
expressed genes (ratio)
Neural cells
Blood 0.69%
Mesoderm 1.03%
Skin 0.46%
E
female
male
F
e9.5
e10.5
e11.5
e12.5
e13.5
Replicate
1
2
3
G
e13.5
e12.5
e11.5
e10.5
e9.5
Neural progenitor
Neuron
Mesoderm
Null
Sox2
Lmx1a
Msx1
Msx2
Pax3
Wnt1
Olig3
Irx3
Irx5
Pax6
Pax7
Gsx2
Ascl1
Gbx2
Gsx1
Dbx2
Dbx1
Sp8
Nkx6-2
Prdm12
Nkx6-1
Foxn4
Olig2
Nkx2-2
Nkx2-9
Foxa2
Ferd3l
Arx
Shh
Lmx1b
Tubb3
Elavl3
Pou4f1
Lhx2
Lhx9
Barhl1
Barhl2
Atoh1
Foxd3
Lhx1
Lhx5
Isl1
Tlx3
Prrxl1
Otp
Pax8
Lbx1
Pax2
Gbx1
Bhlhe22
Ptf1a
Dmrt3
Wt1
Evx1
Evx2
Pitx2
En1
Lhx3
Vsx2
Sox14
Sox21
Vsx1
Tal1
Gata2
Gata3
Isl2
Mnx1
Slc10a4
Slc18a3
Aldh1a2
Arhgap36
Sim1
Sox17
Fermt3
Klf1
Hemgn
Car2
Foxc1
Foxc2
Twist1
Twist2
Meox1
Meox2
Myog
Sox10
Tlx2
Six1
Krt8
Blood
Neural crest
Dorsal root ganglia
Skin

Figure S1: Further characterization of the single cell transcriptome dataset.
(A) Number of cells per replicate and timepoint.
(B) Number of genes per cell for each replicate.
(C) Number of unique molecular identifiers (UMIs) per cell for each replicate.
(D) Ratio of blood (Sox17, Fermt3, Klf1, Hemgn, Car2), mesoderm (Foxc1, Foxc2, Twist1, Twist2, Meox1, Meox2) and skin (Krt8) markers expressed in neural cells.
(E,F) tSNE-plots showing the distribution of male and female cells in the dataset (E), and the different replicates per timepoint (F).
(G) Heatmap showing read distributions of the genes used to assign cell identities to the single cell transcriptomic profiles. Boxed regions indicate the cell identities in which the respective gene is expected to be expressed. Bars at the top of the heatmap indicate sample age (grey early, late red), and cell identity as color coded in Fig 1.

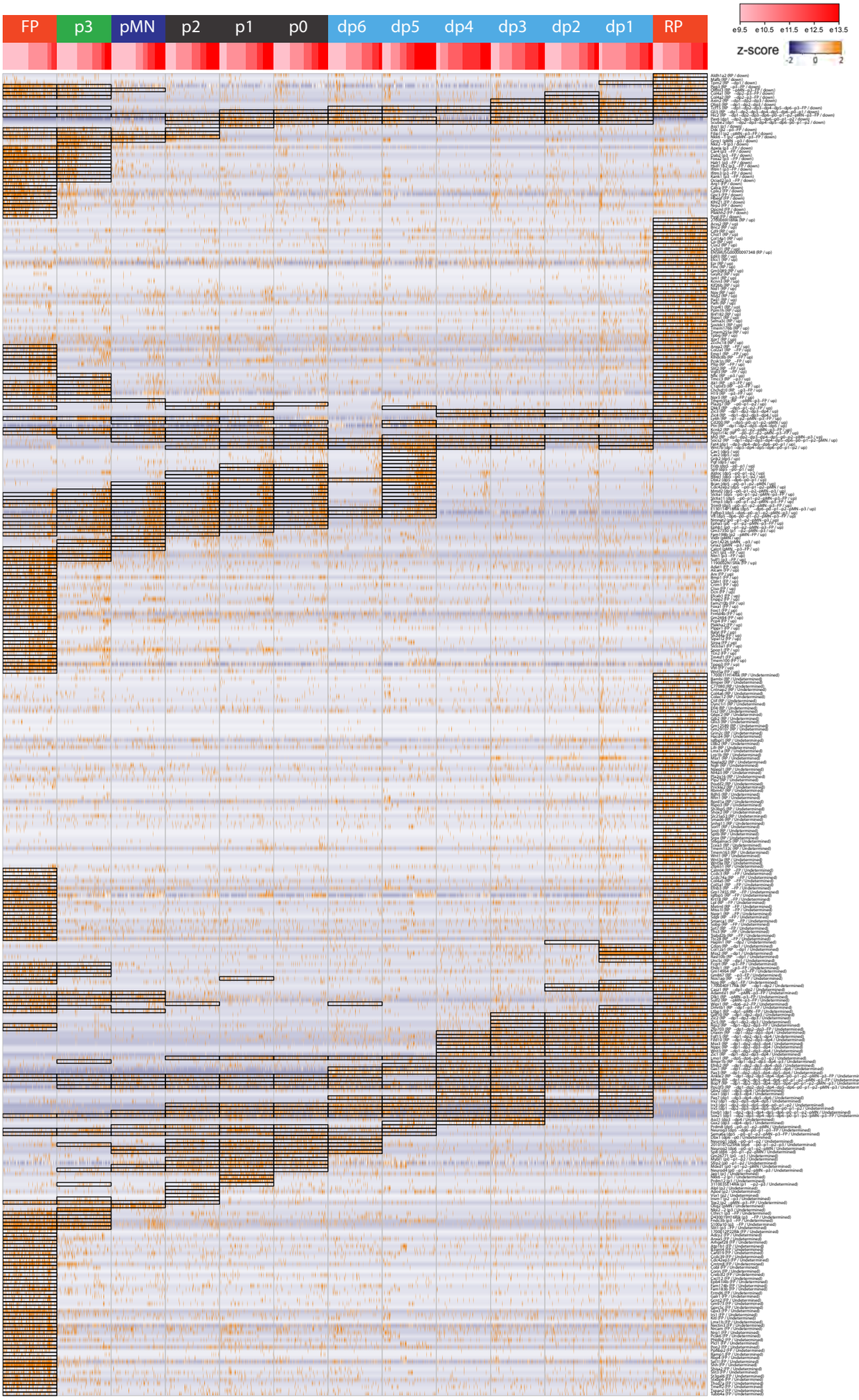
FP
p3
pMN
p2
p1
p0
dp6
dp5
dp4
dp3
dp2
dp1
RP
e9.5
e10.5
e11.5
e12.5
e13.5
z-score
-2
0
2

Figure S2: Differentially expressed genes between the different neural progenitor domains.
Heatmap showing z-scored UMI count distributions of the genes identified as differentially expressed. Domains predicted to express a gene are indicated by boxes. Cells within each domain are ordered by sample time. Rows are ordered according to the correlation between gene expression and sample time (first downregulated genes, $r < -.2$, then upregulated genes, $r > .2$, and finally undetermined trends).
.

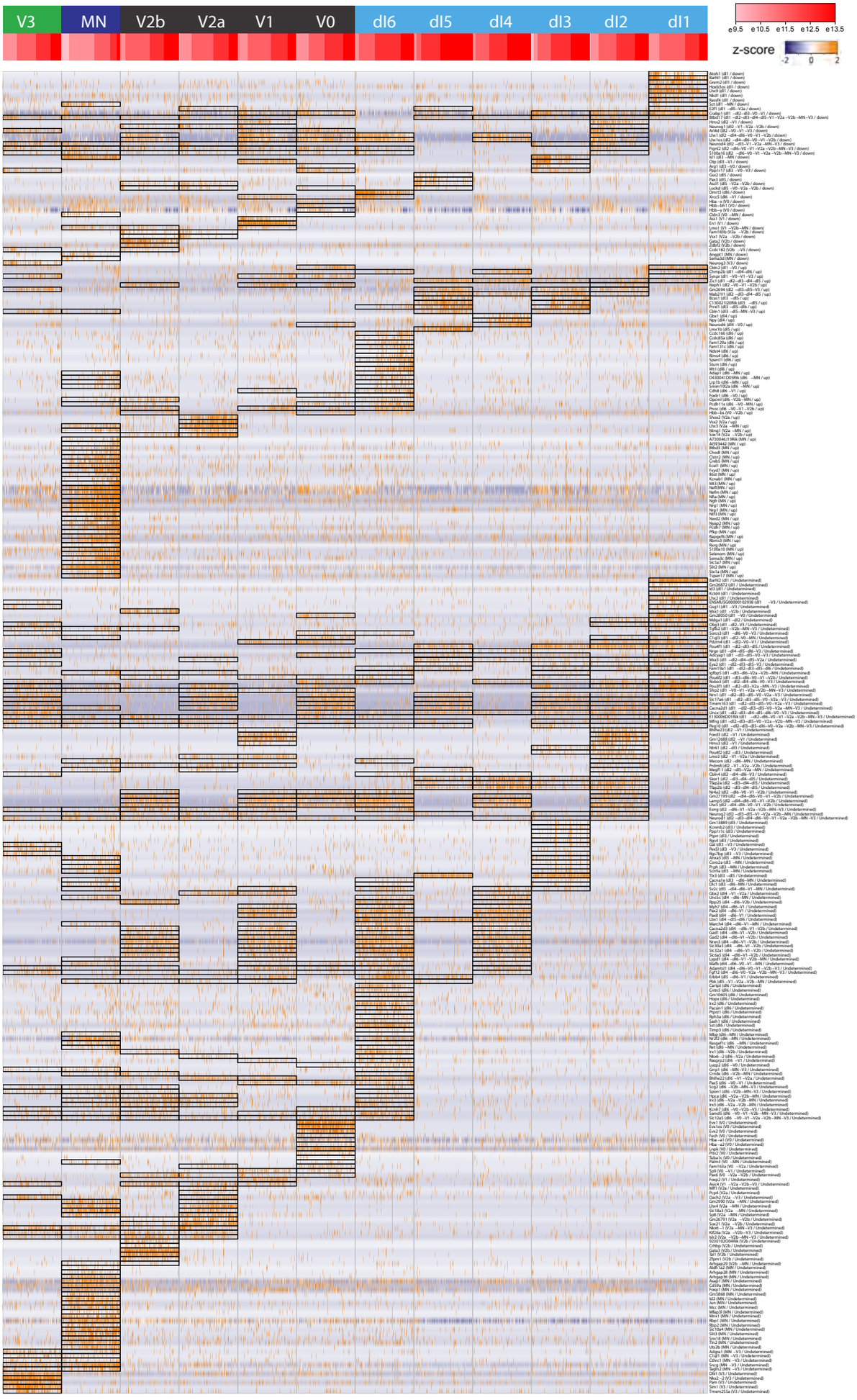
V3
MN
V2b
V2a
V1
V0
dI6
dI5
dI4
dI3
dI2
dI1
e9.5
e10.5
e11.5
e12.5
e13.5
z-score
-2
0
2

Figure S3: Differentially expressed genes between the different neuronal domains.
Heatmap showing z-scored UMI count distributions of the genes identified as differentially expressed. Domains predicted to express a gene are indicated by boxes. Cells within each domain are ordered by sample time. Rows are ordered according to the correlation between gene expression and sample time (first downregulated genes, $r < -.2$, then upregulated genes, $r > .2$, and finally indeterminant trends).

.

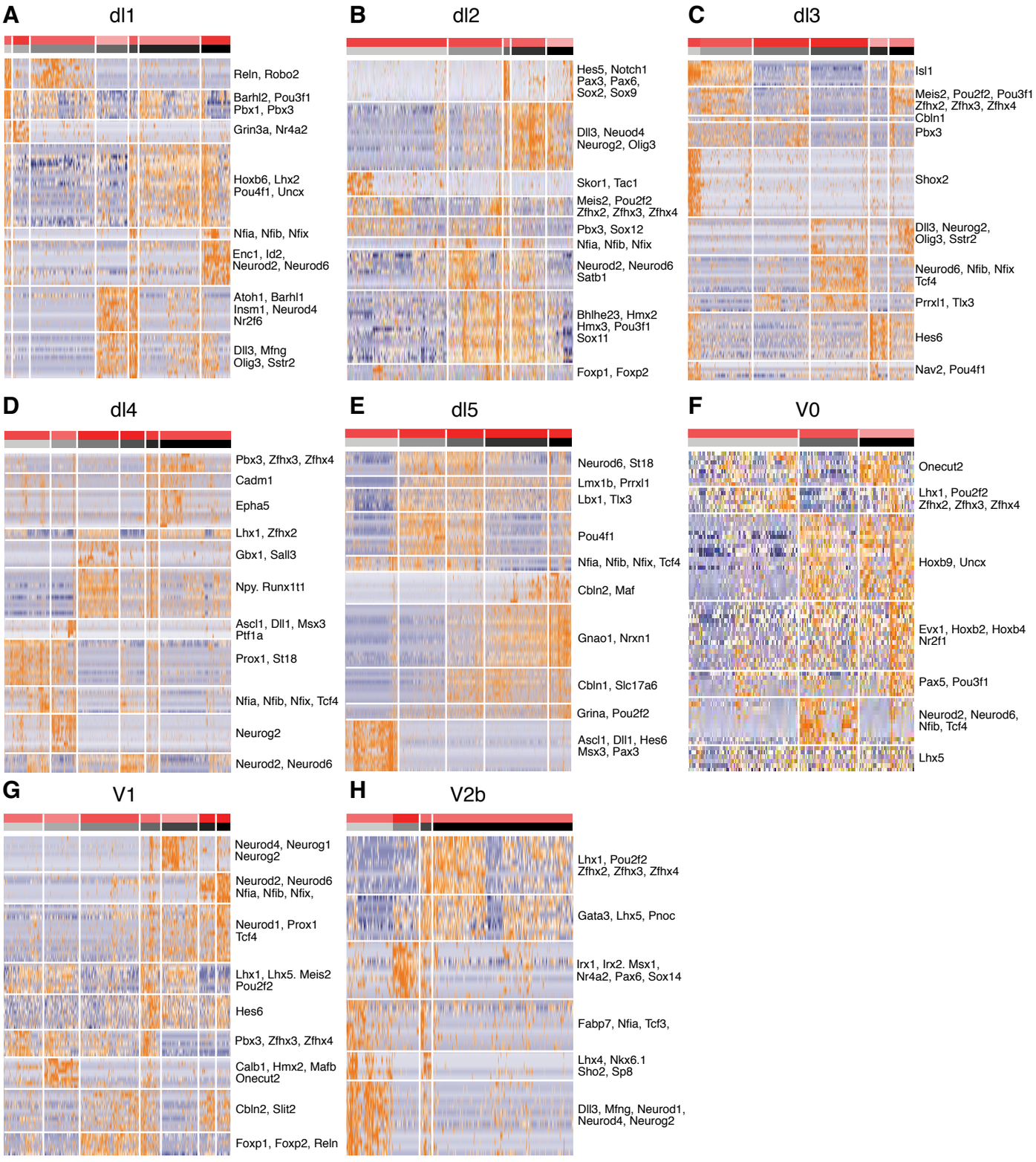

Figure S4: Hierarchical clustering of dI1, dI2, dI3, dI4, dI5, V0, V1 and V2b neurons.
Characterization of neuronal subtypes by hierarchical clustering of the indicated domains. Hierarchical clustering was performed using the curated gene modules available in Table S2. A subset of genes included in the modules are indicated on the righthand side.

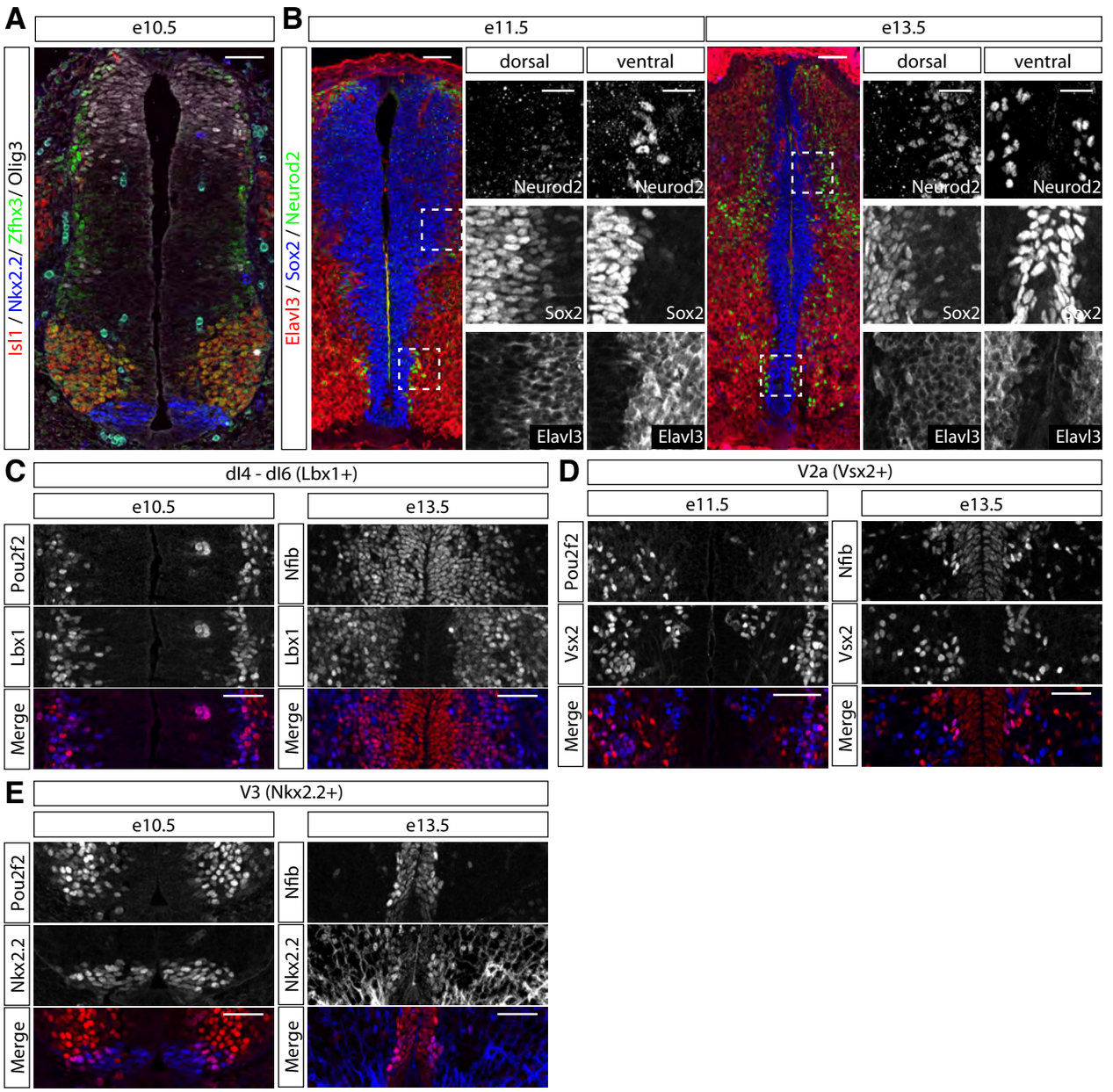

Figure S5: Temporal stratification of neuronal subtypes by a shared set of TFs

(A) Expression of Zfhx3 in neurons at e10.5

(B) Increased expression of Neurod2 in neurons after e11.5. At e11.5 only few neurons in the very dorsal and ventral spinal cord express Neurod2. Number of Neurod2 positive neurons strongly increases between e11.5 and e13.5.

(C-E) Coexpression of Pou2f2 with specific markers for multiple domains at early developmental stages (e10.5 for Nkx2.2 and Lbx1, e11.5 for Vsx2). At e13.5, Nfib is expressed in the same domains in a subset of neurons. These neurons are typically adjacent to the ventricular zone, consistent with their late birth date.

Scale bars = 50 μm, scale bars of insets are 25 μm

.

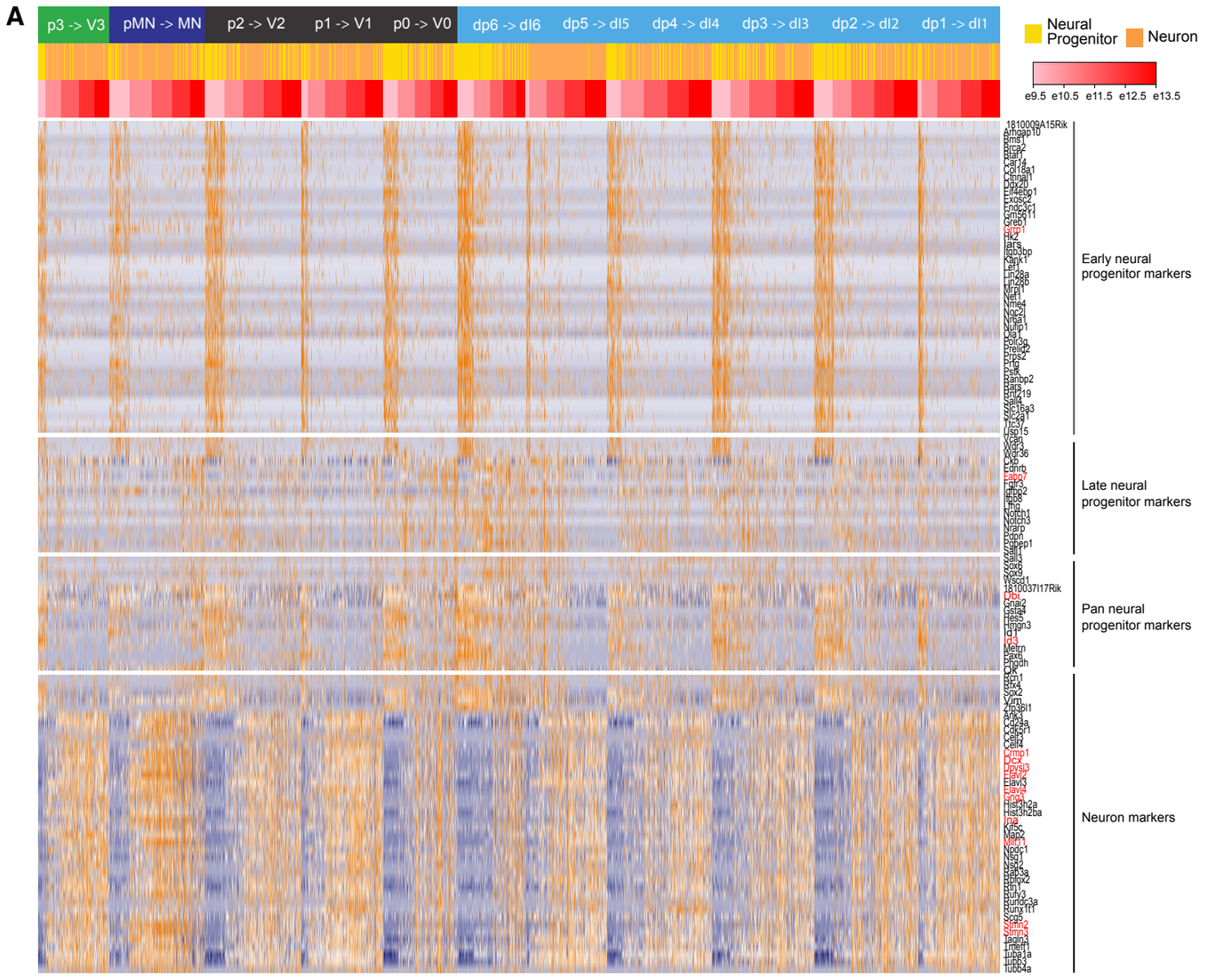

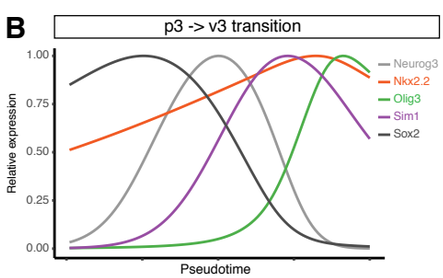

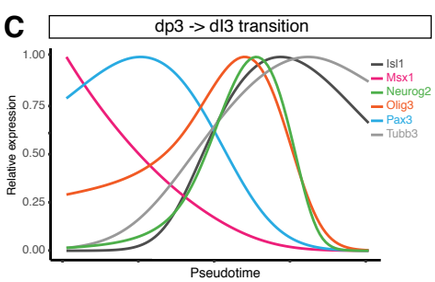

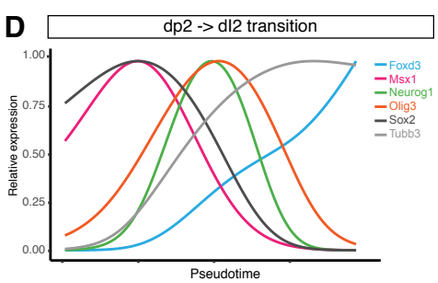

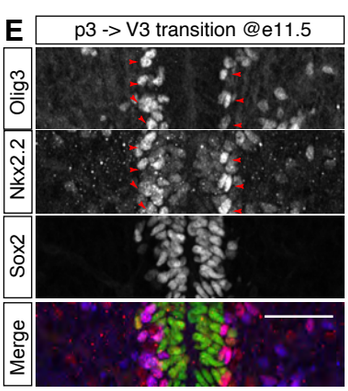

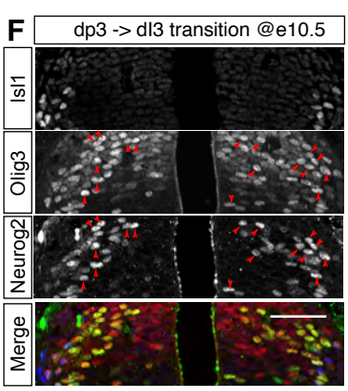

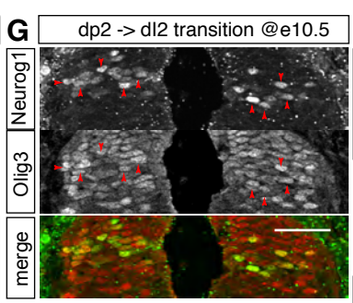

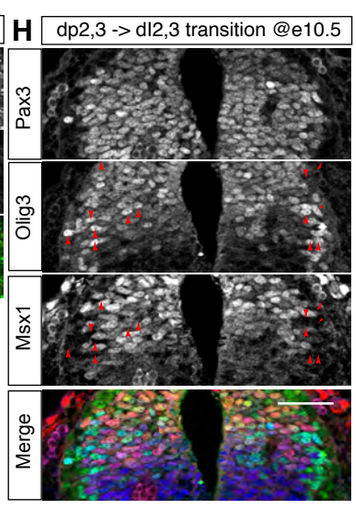

Figure S6: Pseudotime analysis reveals gene expression dynamics underlying neurogenesis in several domains.

(A) Heatmap showing the 4 genes modules identified as similarly expressed in all dorsal-ventral domains and involved in neurogenesis and progenitor maturation. Among the 114 genes, red gene labels indicate genes excluded from the following analysis because of significant dorsal-ventral bias.
(B) Smoothed expression profile of the neurogenic trajectory from p3 to V3 shows increasing levels of Nkx2.2 during neurogenesis. Note that Nkx2.2 in contrast to other neural progenitor markers continues to be expressed in V3 neurons.
(C) Smoothed expression profile of the neurogenic trajectory from dp3 to dI3 shows a transient upregulation of Olig3 prior to neurogenesis that coincides with the maximal expression of Neurog2.
(D) Smoothed expression profile of the neurogenic trajectory from dp2 to dI2 shows a transient upregulation of Olig3 prior to neurogenesis that coincides with the maximal expression of Neurog1.
(E) Upregulation of Nkx2.2 in Olig3+ (red arrows) V3 neurons compared to Sox2+ Nkx2.2 p3 progenitors at e11.5.
(F) Upregulation of Olig3 in neurogenic dp3 progenitors labelled by Neurog2 (red arrows).
(G) Upregulation of Olig3 in neurogenic dp2 progenitors labelled by Neurog1 (red arrows).
(H) Specific upregulation of Olig3 is anti-correlated with Msx1 (red arrows). The broadly dorsal progenitor marker Pax3 is homogeneously expressed in dp2 and dp3 domains.
Scale bars = 50 μm

SUPPLEMENTAL TABLES

Table S1. Knowledge matrix used to identify cell types. Columns indicate the cell type classes and rows the genes. A gene contributes to a class definition if the associated value is 1.

Click here to Download Table S1

Table S2. Curated gene lists used to cluster the neuronal subtypes in each dorsal-ventral domain.

Click here to Download Table S2

Table S3. List of primary antibodies including manufacturer and the dilutions used.

Click here to Download Table S3

Table S4. Summary table indicating the number of genes and modules for each step of the gene module identification method used to cluster the neuronal subtypes.

Click here to Download Table S4